



140
475
THS

1
2007



This is to certify that the
thesis entitled

MICROCAVITY POLARITONS IN QUANTUM DOT LATTICES

presented by

ERIC MATTHIAS KESSLER

has been accepted towards fulfillment
of the requirements for the

 M.S. degree in PHYSICS AND ASTRONOMY

A handwritten signature in cursive script, appearing to read "John Pennoyer", written over a horizontal line.

Major Professor's Signature

 7/12/2007

Date

**MICROCAVITY POLARITONS IN QUANTUM DOT
LATTICES**

By

Eric Matthias Kessler

A THESIS

Submitted to
Michigan State University
in partial fulfillment of the requirements
for the degree of

MASTER OF SCIENCE

Department of Physics and Astronomy

2007

ABSTRACT

MIROCAVITY POLARITONS IN QUANTUM DOT LATTICES

By

Eric Matthias Kessler

Exciton-polaritons are mixed modes resulting from the strong coupling of electron-hole pairs in a semiconductor (excitons) and photons. In this thesis, the exciton-polariton modes of a quantum dot lattice embedded in a planar optical microcavity are studied. Due to the symmetry mismatch of the exciton state in the discrete lattice with the continuous two dimensional photon modes, each exciton mode couples to many cavity field modes. These additional coupling terms do not conserve momentum and are called “umklapp” terms.

We provide a complete derivation of the system’s Hamiltonian, which is subsequently investigated both by analytical and numerical methods. We focus our analysis on novel polaritons appearing at the edge of the Brillouin zone in the reciprocal space. The large in-plane momentum of these polaritons can give rise to a total internal reflection, which is expected to greatly enhance their spontaneous emission lifetime. We show that at certain symmetry points in the Brillouin zone both of a square and a hexagonal QD lattice this new kind of polaritons can be considered as nearly bosonic quasiparticles with an exceptionally small, isotropic mass of the order of 10^{-8} electron masses (m_0), much smaller than both the exciton mass ($\sim 0.5 m_0$) and the cavity photon mass ($\sim 10^{-5} m_0$). Polaritons with positive as well as negative masses are found. The large lifetime and the extremely small mass suggest interesting possibilities for the observation of polariton condensation effects.

ACKNOWLEDGMENTS

I would like to thank my advisor Professor Carlo Piermarocchi for his great support in the past year.

TABLE OF CONTENTS

LIST OF TABLES	v
LIST OF FIGURES	vi
Introduction	1
1 Core Concepts	5
1.1 Wannier-Mott Exciton Theory	6
1.2 Polariton Theory	12
1.3 Confined Excitons	16
2 The Model	21
2.1 The Hamiltonian	22
2.1.1 The Exciton Hamiltonian	22
2.1.2 The Photon Hamiltonian	26
2.1.3 Exciton-Photon Interaction	28
2.2 Analysis of the full Hamiltonian	32
2.2.1 Simplifications and Approximations	34
2.2.2 The Exciton at Resonance and the Strong Coupling Regime	37
3 Numerical Calculation	41
3.1 Preliminary Discussion	43
3.2 Square Lattice: The X-Point	46
3.3 Square Lattice: The M-Point	52
3.4 Hexagonal Lattice: The W-Point	58
3.5 Dark Polariton States	62
Conclusion	66
APPENDICES	72
A Derivation of the Effective Mass Equation in Bulk	72
B Evaluation of the Interaction Matrix Element	75
BIBLIOGRAPHY	80

LIST OF TABLES

3.1	The Rabi splitting Ω depends on the relative size of the wave vector \tilde{d} at the crossing point and the number of intersecting modes.	46
3.2	The effective masses for the upper two polariton modes at X. The masses are expressed in units of the photon effective mass in a ideal cavity of length $L = 0.171 \mu\text{m}$ ($m_{ph} = 2.52 \cdot 10^{-5} m_0$).	48
3.3	The effective masses for the upper (UP) and the lower polariton (LP) at M1 and M2. The masses are expressed in units of the photon effective mass in a ideal cavity of length $L = 0.171 \mu\text{m}$ ($m_{ph} = 2.52 \cdot 10^{-5} m_0$).	56

LIST OF FIGURES

1.1	The conduction and valence band of the semiconductor with a direct bandgap of size Δ	7
1.2	In the two particle picture the exciton states are found to be in the gap between zero energy and the uncorrelated electron-hole energies (shaded area). $E_1(\mathbf{q})$ is the exciton energy of the first excited exciton state given in Eq. (1.21).	11
1.3	The Polariton dispersion. The dashed lines are the exciton and photon dispersions without interaction. Note that this sketch is not to scale.	16
1.4	The exciton and photon shares, $u_{\mathbf{k}}^1$ and $v_{\mathbf{k}}^1$ of the upper polariton mode	16
1.5	In zeroth order the bandstructure varies spatially like a step function at the edge of two semiconductors	17
2.1	N identical quantum dots of disc-like shape in an ideal periodic array embedded in a planar microcavity.	21
2.2	The quantum dots we are considering have a cylindrical, disc-like shape. The thickness of the dot is labelled by L_z and the radius by R_0	22
2.3	The in-plane dispersion modes (n=1,2,3) of a microcavity. The dashed line is the two dimensional dispersion of a free photon.	27
2.4	In the quantum well case there is a one to one correspondence of states in the exciton-photon interaction (a), whereas the quantum dot exciton couples to a continuous photon bath (b). The QD lattice presents an intermediate case, where the exciton couples to a infinite but discrete set of photon modes (c). In the latter two cases the coupling for large \mathbf{q} is suppressed by the form factor $\tilde{\chi}(\mathbf{q})$	33
2.5	The first four photon modes in the reduced zone scheme.	34
3.1	The reciprocal lattice:(a) of a square lattice with lattice constant a and (b) of a hexagonal lattice with constant a . As usual Γ denotes the origin $\mathbf{q} = 0$	44
3.2	The function $f(\beta, L)$. The light regions correspond to higher values.	45

3.3	Plot of the derivative of $f(R_0/\sqrt{2}, L)$ with respect to L for a fixed $R_0 = 50$ nm. Notice that the coupling is maximal for a value of $L = 0.171 \mu\text{m}$	45
3.4	The polariton modes (1)-(3) at the X-point along $\overline{\Gamma X}$ (a) and along \overline{XM} (b). The upper polariton (1) has a local minimum and can thus be considered as a quasiparticle with a positive effective mass. The dashed lines represent the unperturbed modes.	47
3.5	The upper polariton dispersion at the X-point. Because of the special π -rotational symmetry of this point the dispersion has a valley at the edge of the Brillouin zone.	48
3.6	The exciton component of polariton mode (1) $ \alpha_x^{(1)}(\mathbf{q}) ^2$. Only in the direct vicinity of \mathbf{q}_0 the upper polariton becomes excitonic.	49
3.7	The exciton component of mode (2) $ \alpha_x^{(2)}(\mathbf{q}) ^2$. Remarkably this mode is purely photonic on the edge of the Brillouin zone.	50
3.8	The exciton component of mode (3) $ \alpha_x^{(3)}(\mathbf{q}) ^2$. At resonance this mode is half excitonic half photonic.	51
3.9	At the M point we distinguish two cases. M1 labels the crossing, where the closest photon modes intersect (black dots). At the M2 crossing the second closest photon modes intersect (crosses). The different modes fulfill $ \mathbf{Q}_i + \mathbf{q}_0 = d_{1/2}$ for the two cases, respectively.	52
3.10	The polariton modes at the lowest crossing point at M (M1). The modes are displayed along the path $\overline{\Gamma M}$	53
3.11	The polariton modes at the lowest crossing point at M. The modes are displayed along a path parallel to the q_x -axis. Due to the symmetry we find the same energy dispersions along the q_y -axis	53
3.12	The upper polariton mode at M1. The energy dispersion is symmetric in q_x -and q_y -direction.	54
3.13	The exciton component of mode (1) at M1 $ \alpha_x^{(1)}(\mathbf{q}) ^2$. At resonance this mode is half excitonic half photonic. An almost identical figure is found in the case of the lower polariton (5).	55

3.14	At M2 eight photon modes are crossing. The resulting nine polariton modes are displayed along the q_x -direction. Note that along this path the unperturbed photon modes can be grouped in degenerate pairs.	56
3.15	The highest polariton mode at M2. The large number of interacting photon modes provides a high symmetry of the dispersion.	57
3.16	The exciton component of the highest mode at M2 $ \alpha_x(\mathbf{q}) ^2$. At resonance this mode is half excitonic half photonic. We find an almost identical figure in the case of the LP.	57
3.17	The polariton modes at the W-point of the hexagonal lattice along the x-direction (a) and the y-direction (b) are displayed.	58
3.18	The highest polariton mode at the W-point of the hexagonal lattice.	59
3.19	The exciton component of the highest mode at W in the hexagonal lattice $ \alpha_x(\mathbf{q}) ^2$. At resonance this mode is half excitonic half photonic.	60
3.20	The lowest polariton mode at the W-point of the hexagonal lattice. Note that it is rotated by π with regard to the upper polariton mode.	60
3.21	The exciton component of the lowest mode at W in the hexagonal lattice $ \alpha_x(\mathbf{q}) ^2$. It is rotated by π with regard to the excitonic part of the upper mode.	61
3.22	The dispersion for external photons for several arbitrary values of the (continuous) parameter k_z . The dispersion for $k_z = 0$ imposes a lower boundary for the energies accessible to free photons.	63
3.23	The boundary between states accessible for external photons in the reduced zone scheme for the unperturbed cavity modes in the cases (1) $n_{ext} < \alpha n_r$, (2) $n_{ext} = \alpha n_r$ and (3) $n_{ext} > \alpha n_r$. Moreover, the figure shows the lowest 2 cavity photon modes along \overline{OX} of the square lattice.	64
3.24	If the condition $n_{ext} < \alpha n_r$ is fulfilled there are polariton modes in the dark region (shaded area). These states do not couple to external photons and are thus expected to have a greatly enhanced lifetime.	65

Introduction

Within the broad area of Solid State Physics the physics of semiconductor nanostructures is currently one of the most active research fields. Perhaps, the best examples of novel systems in this blossoming area are given by low dimensional quantum structures such as quantum dots (QD) [36, 37, 38] and quantum wells (QW) [40, 49], which are zero and two dimensional quantum heterostructures, respectively. Tremendous efforts both to engineer and to understand the physics of these low dimensional systems have been made in the last few decades. The elementary electronic excitations of a semiconductor can be treated in a quasiparticle picture. The properties of these quasiparticles, called excitons, depend strongly on the dimensionality of the solid. For instance, the many body behaviour of excitons ranges from an almost purely bosonic behaviour in the bulk and QW case [12] to purely fermionic behaviour in the point-like QD case [50].

The most exciting features of low dimensional semiconductor structures become manifest in the interaction with light. Light trapped in a microcavity - ideally given by two facing mirrors- can strongly couple to excitons giving rise to a new kind of quasiparticle called exciton-polariton [19, 40]. Polaritons are coupled half-matter, half-light states with a photon-like mass - and thus a group velocity close to c - and at the same time the ability to strongly interact with matter, due to their excitonic part. These properties as well as recent advances in the experimental fabrication of semiconductor nanostructures have suggested that polaritons could be applied to the

realization of scalable quantum information devices [51].

The concept of quantum computing was originally proposed by Feynman and others in 1982 [17]. Feynman suggested that it might be impossible to simulate a quantum mechanical system with an ordinary computer without an exponential slowdown in the efficiency of the simulation. A new type of computers, based entirely on the principles of quantum mechanics, would be necessary for these challenging tasks. Nevertheless, it was not until Shor's publication in 1994 [44], where he presented an algorithm that demonstrated the outstanding potential of quantum computing, that this novel field gathered momentum and turned into an active and promising area of research. In a quantum computer the logical units, called qubits, can be realized by impurity spin states or electrons in quantum dots. For the selective entanglement of those states polaritons seem to be excellent candidates. Due to their photon-like mass combined with the ability to interact with matter [35], they can be used as "mediating" particles in order to establishing an effective interaction between the qubit states.

Furthermore, the possible observation of quantum phase transitions in strongly coupled light-matter systems has attracted much attention lately. Polaritons behave in certain limits like a non interacting Bose gas and have an extremely light mass. Therefore they are considered to be suited optimally for the realization of quantum condensed phases in solids. In fact, recently several works have been published claiming the experimental evidence of microcavity exciton-polariton condensation [3, 14, 24]. Disregarding the controversial theoretical discussion about the nature of the observed condensation effects - we will briefly discuss some aspects of that subject at the end of the thesis - the field of polariton quantum condensation is highly interesting because it brings pure quantum effects to a macroscopic scale.

In this thesis we will provide for the first time a theoretical discussion of a system that can be considered as an intermediate case between a quantum well on the one

hand and a single quantum dot on the other. It consists of a periodic array of semiconductor QD's embedded in a planar microcavity. The invariance of the system under translations by an arbitrary lattice vector partially restores the full translational symmetry of a QW, which is completely destroyed in the single QD case.

Chapter 1 starts with a review of the theoretical core concepts of the physics of semiconductor nanostructures. We will provide a quantum mechanical treatment of excitons in QW's as well as in confined structures like QD's and discuss their many body behaviour in these two cases. Furthermore, we will study the exciton-photon interaction and present the polariton concept by introducing the Hopfield transformations.

In Chapter 2, we will focus on the physics of the system under consideration, which consists of a QD lattice in a semiconductor microcavity. We will see that the exciton center-of-mass motion in the lattice is quantised and it can be characterized by a quantum number \mathbf{q} , restricted to the first Brillouin zone, which we identify as the exciton in-plane momentum. In this in-plane motion the exciton behaves like a quasiparticle with infinite mass. In the interaction with light the quantized in-plane motion of the exciton gives rise to a quasi-momentum conservation. Unlike the case of a QW, there is not a one to one correspondence of an exciton mode with a photon mode in the exciton-photon interaction, but an exciton with momentum \mathbf{q} couples to a discrete and yet infinite set of photons with in-plane wave vector $\mathbf{q} + \mathbf{Q}$, where \mathbf{Q} denotes an reciprocal lattice vector. Due to the finiteness of the quantum dot size, the coupling to photon states with large momentum is suppressed by an exponential factor, so that the set of photons has effectively a finite size. The chapter ends with some preliminary considerations on the numerical calculations of Chapter 3

In Chapter 3, we will finally present the numerical calculations of the polariton modes in our system. At certain symmetry points of the reciprocal lattice the polariton can be considered as a quasiparticle with an exceptionally small and isotropic

mass, which is smaller than the mass for QW polaritons by a factor of 10^{-3} . We will study these novel kind of polaritons in a square and a hexagonal lattice at several special symmetry points of the reciprocal space. Furthermore, we will see that in our system polaritons with large in-plane momentum can be created. This is in contrast with the QW case, where the polariton momentum is always close to zero due to the steep photon dispersion. This large in-plane momentum can give rise to a total internal polariton reflection in the microcavity, which is expected to dramatically increase the spontaneous emission lifetime of the QD lattice polaritons.

The thesis ends with comments on possible applications of this novel system and future directions of research that may expand the investigations presented in this thesis.

CHAPTER 1

Core Concepts

By definition a polariton is an excitation that arises from the coupling of an electromagnetic wave with the elementary excitations of a crystal, like for examples phonons, plasmons, excitons, magnons, but also coupled excitation modes like phonon-plasmons, etc. In the further discussion we will focus on the case of exciton-polaritons, i.e. the coupling of an electronic crystal excitation, the exciton, and the radiation field.

In the description of polaritons there are two different ways to address the problem. On the one hand there is the semiclassical, macroscopic point of view, and on the other hand there is the purely quantum mechanical, microscopic treatment. In the macroscopic picture the electromagnetic wave propagates inside the crystal, which reacts to the external fields according to a linear response theory. This response of the crystal due to the electromagnetic field gives rise to a dielectric constant, that finally alters the dispersion relation of the propagating wave. These altered electromagnetic modes are nowadays called polariton modes, although the name polariton (a combination of polarisation and photon) had not been introduced until 1958 when Hopfield established the quantum mechanical treatment of this issue [20].

Hopfield introduced the concept of polaritons, which are the normal modes of a system of 2 coupled oscillations, namely the photon and the crystal excitation. Although similar ideas have been discussed earlier by Fano [16] and by Born and Huang

[5, 21], Hopfield was the first one to realize that the classical picture of electromagnetic radiation interacting with matter, in which the wave is partially absorbed and partially propagates inside the specimen, must be fundamentally reviewed.

In his new idealised picture only polaritons exist inside the crystal. A photon on the crystal surface can give rise to a polariton which propagates inside the crystal until it arrives at another surface or decays, e.g. due to scattering processes. In the following we are going to describe this quantum mechanical picture of a bulk semiconductor crystal coupled to photons. We assume excitons to be the only excitations of the crystal, which is a good approximation in the vicinity of the exciton resonance frequency.

1.1 Wannier-Mott Exciton Theory

According to the effective mass equation (which we will derive later) excitons are quasiparticles in a solid that can be considered as a hydrogenic bound state of an excited electron in the conduction band and the remaining hole in the valence band.

In this chapter we will review the theory of Wannier-Mott excitons. In contrast to the so called Frenckel exciton the W-M exciton has a Bohr radius much larger than the interatomic spacing of the crystal.

The kind of excitons in a solid is determined by the properties of the material under consideration, in particular by the value of the dielectric constant. Typically, the type of exciton in inorganic semiconductors is the Wannier-Mott exciton due to the large dielectric constant, which leads to a screening of the effective electron-hole interaction and thus to a large Bohr radius.

Starting from first principles, an exciton is an excitation of the whole electron many body system in the crystal including the electron-electron interaction. For simplicity we only consider the valence and conduction band of the semiconductor and we assume a quadratic dispersion for valence and conduction band electrons, as

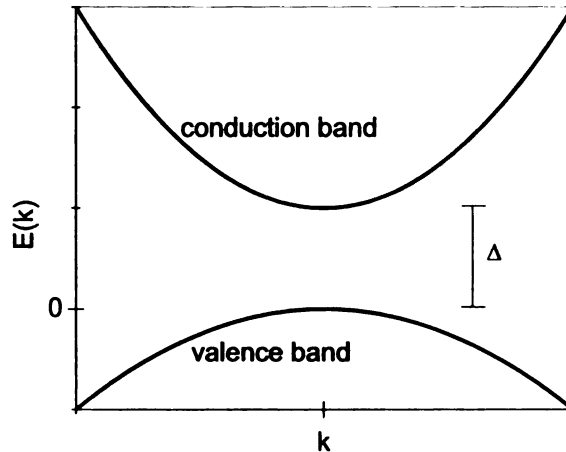


Figure 1.1. The conduction and valence band of the semiconductor with a direct bandgap of size Δ .

well as a direct bandgap of size Δ (Fig. 1.1).

In this choice the single electron energies in valence and conduction band are:

$$E_v(\mathbf{k}) = -\frac{\hbar^2 k^2}{2m_v}, \quad E_c(\mathbf{k}) = \Delta + \frac{\hbar^2 k^2}{2m_c}. \quad (1.1)$$

Here, m_c and $-m_v$ are the effective masses of conduction and valence electrons, respectively. So, in second quantisation, the Hamiltonian without interaction, H_0 , takes the form

$$H_0 = \sum_{\mathbf{k}} \left(E_v(\mathbf{k}) c_{v\mathbf{k}}^\dagger c_{v\mathbf{k}} + E_c(\mathbf{k}) c_{c\mathbf{k}}^\dagger c_{c\mathbf{k}} \right), \quad (1.2)$$

where $c_{c/r\mathbf{k}}^\dagger$ and $c_{c/r\mathbf{k}}$ are the creation and annihilation operators for Bloch electrons in the valence and conduction band, respectively:

$$\langle \mathbf{r} | c_{\sigma\mathbf{k}}^\dagger | 0 \rangle = \langle \mathbf{r} | \sigma\mathbf{k} \rangle = \frac{1}{\sqrt{V}} e^{i\mathbf{k}\mathbf{r}} u_{\sigma\mathbf{k}}(\mathbf{r}). \quad (1.3)$$

The development in the completely delocalized Bloch functions rather than in the localized Wannier functions turns out to be convenient for the description of weakly bound, i.e. Wannier-Mott excitons.

As the intraband interaction of electrons does not affect excitations in the optical frequency range we are considering here [13], we exclusively take into account the interaction between valence and conduction electrons. The general form for such an interband interaction is

$$H_I = \sum_{\mathbf{k}_1 \mathbf{k}_2 \mathbf{k}_3 \mathbf{k}_4} f_{\mathbf{k}_1 \mathbf{k}_2 \mathbf{k}_3 \mathbf{k}_4} c_{v\mathbf{k}_1}^\dagger c_{c\mathbf{k}_2}^\dagger c_{c\mathbf{k}_3} c_{v\mathbf{k}_4}. \quad (1.4)$$

Note, that we did not take into account spin interaction and therefore dropped the related index.

In the usual approximation [25] the matrix element $f_{\mathbf{k}_1 \mathbf{k}_2 \mathbf{k}_3 \mathbf{k}_4} = \langle \mathbf{k}_1 v, \mathbf{k}_2 c | \hat{V} | \mathbf{k}_3 c, \mathbf{k}_4 v \rangle$, which arises from the repulsive Coulomb interaction between electrons, can be evaluated as

$$f_{\mathbf{k}_1 \mathbf{k}_2 \mathbf{k}_3 \mathbf{k}_4} = \frac{4\pi e^2}{\epsilon V} \frac{1}{|\mathbf{k}_1 - \mathbf{k}_4|^2} \delta_{\mathbf{k}_1 - \mathbf{k}_4, \mathbf{k}_3 - \mathbf{k}_2}, \quad (1.5)$$

where ϵ is a finite dielectric constant due to the effective screening of all not explicitly included charges (electrons and ions) and V is the quantisation volume.

Hence, we can write the total exciton Hamiltonian as

$$\begin{aligned} H_x &= H_0 + H_I \\ &= \sum_{\mathbf{k}} \left(\Delta + \frac{\hbar^2 k^2}{2m_c} \right) c_{c\mathbf{k}}^\dagger c_{c\mathbf{k}} - \sum_{\mathbf{k}} \frac{\hbar^2 k^2}{2m_v} c_{v\mathbf{k}}^\dagger c_{v\mathbf{k}} \\ &\quad + \sum_{\mathbf{k}_1 \mathbf{k}_2 \mathbf{k}_3 \mathbf{k}_4} \frac{4\pi e^2}{\epsilon V} \frac{1}{|\mathbf{k}_1 - \mathbf{k}_4|^2} c_{v\mathbf{k}_1}^\dagger c_{c\mathbf{k}_2}^\dagger c_{c\mathbf{k}_3} c_{v\mathbf{k}_4} \delta_{\mathbf{k}_1 - \mathbf{k}_4, \mathbf{k}_3 - \mathbf{k}_2}. \end{aligned} \quad (1.6)$$

The subsequent step is to diagonalize this Hamiltonian. The ground state of the system can be found by occupying all electron states in the valence band

$$|\Phi_0\rangle = \prod_{\mathbf{k}} c_{v\mathbf{k}}^\dagger |0\rangle. \quad (1.7)$$

It is straightforward to verify that this state is an eigenstate with eigenvalue

$$E_0 = \sum_{\mathbf{k}} E_v(\mathbf{k}). \quad (1.8)$$

In order to find the other eigenstates we define a trial excited state as a superposition of all possibilities to promote one electron from valence to conduction band:

$$|\Psi\rangle = \sum_{\mathbf{k}\mathbf{k}'} A(\mathbf{k}, \mathbf{k}') c_{c\mathbf{k}}^\dagger c_{v\mathbf{k}'} |\Phi_0\rangle \quad (1.9)$$

It turns out to be convenient to introduce new variables, namely

$$\mathbf{K} = \frac{m_c \mathbf{k}' + m_v \mathbf{k}}{M} \quad (1.10)$$

$$\mathbf{q} = \mathbf{k} - \mathbf{k}'. \quad (1.11)$$

In this choice (1.9) becomes:

$$|\Psi\rangle = \sum_{\mathbf{q}\mathbf{K}} A_{\mathbf{q}}(\mathbf{K}) c_{c, \mathbf{K} + (m_c/M)\mathbf{q}}^\dagger c_{v, \mathbf{K} - (m_v/M)\mathbf{q}} |\Phi_0\rangle, \quad (1.12)$$

where we have changed the summation index and renamed the coefficients

$A_{\mathbf{q}}(\mathbf{K}) := A(\mathbf{K} + (m_c/M)\mathbf{q}, \mathbf{K} - (m_v/M)\mathbf{q})$. This choice is strictly not necessary, but turns out to be useful, as it transforms the electron-hole system in the center of mass frame.

Now we try to determine the coefficients $A_{\mathbf{q}}(\mathbf{K})$ in such a way that $|\Psi\rangle$ is an eigenstate of the Hamiltonian (1.6). From the stationary Schrödinger equation

$$H |\Psi\rangle = E |\Psi\rangle \quad (1.13)$$

we find by applying the Fermi commutation relations for the electron operators

$$\left[c_{v(c)\mathbf{k}}, c_{v(c)\mathbf{k}'}^\dagger \right]_+ = \delta_{\mathbf{k}, \mathbf{k}'}, \quad (1.14)$$

that the coefficients obey the so called *effective mass equation* (EME) in momentum space representation

$$\left[-\tilde{E} + \frac{\hbar}{2\mu} K^2 + \frac{\hbar}{2M} q^2 \right] A_{\mathbf{q}}(\mathbf{K}) + \sum_{\mathbf{K}'} \frac{4\pi e^2}{V\epsilon} \frac{1}{|\mathbf{K} - \mathbf{K}'|^2} A_{\mathbf{q}}(\mathbf{K}') = 0, \quad (1.15)$$

where $M = m_c + m_v$ and $\mu = \frac{m_v m_c}{m_v + m_c}$ are the total mass and the reduced mass, respectively and $\tilde{E} = E - E_0 - \Delta$. The complete derivation of the EME is given in Appendix A.

Eq. (1.15) tells us that coefficients with different \mathbf{q} are decoupled, which makes \mathbf{q} a good quantum number to label the eigenstates. In this spirit we find the exciton states to be of the form

$$|\Psi_{\mathbf{q}}\rangle = \sum_{\mathbf{K}} A_{\mathbf{q}}(\mathbf{K}) c_{c, \mathbf{K} + (m_c/M)\mathbf{q}}^\dagger c_{v, \mathbf{K} - (m_v/M)\mathbf{q}} |\Phi_0\rangle. \quad (1.16)$$

If we now Fourier transform the coefficients in (1.15)

$$\Psi(\mathbf{r}, \mathbf{R}) = \frac{1}{V} \sum_{\mathbf{q}, \mathbf{K}} A_{\mathbf{q}}(\mathbf{K}) e^{i(\mathbf{q}\mathbf{R} + \mathbf{K}\mathbf{r})}, \quad (1.17)$$

we realize that Eq. (1.15) is equivalent to the Schrödinger equation of 2 particles of positive masses m_c and m_v in an attractive Coulomb potential in the center of mass frame, which is the *effective mass equation* for excitons in real space representation:

$$\left(-\frac{\hbar^2}{2M} \nabla_{\mathbf{R}}^2 - \frac{\hbar^2}{2\mu} \nabla_{\mathbf{r}}^2 - \frac{e^2}{\epsilon r} \right) \Psi = \tilde{E} \Psi. \quad (1.18)$$

This is a remarkable result. The problem of solving the Schrödinger equation for the intricate Hamiltonian (1.6) reduces to the elementary problem of two particles in an attractive Coulomb potential. Naturally we interpret this result in the manner that the promoted electron enters a hydrogenic bound state with the remaining hole in the valence band. In that interpretation \mathbf{q} is the total momentum of the electron hole system, which is conserved in our idealised model and thus a good quantum number to label the exciton eigenstates.

We should mention that the effective mass equation can be derived from first principles and taking into account the full electron-electron interaction [43]. By using a Green's-function formalism, Eq. 1.18 can be obtained in the lowest order approximation to the effective electron-hole interaction.

Eq. (1.18) has the well known solutions

$$\Psi_{\mathbf{q}, n}(\mathbf{R}, \mathbf{r}) = e^{i\mathbf{q}\mathbf{R}} \Phi_n(\mathbf{r}), \quad \tilde{E}_{\mathbf{q}, n} = \frac{\hbar^2 q^2}{2M} - \frac{\mu c^4}{2\epsilon^2 \hbar^2 n^2}, \quad (1.19)$$

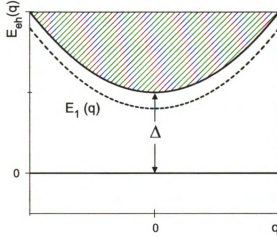


Figure 1.2. In the two particle picture the exciton states are found to be in the gap between zero energy and the uncorrelated electron-hole energies (shaded area). $E_1(\mathbf{q})$ is the exciton energy of the first excited exciton state given in Eq. (1.21).

where $\phi_n(\mathbf{r})$ are the atomic orbital states of the hydrogen problem.

With the choice $E_0 = 0$ we have finally found the eigenstates and energies of the exciton Hamiltonian to be

$$|\Psi_{\mathbf{q}}^n\rangle = \sum_{\mathbf{K}} A_{\mathbf{q}}^n(\mathbf{K}) c_{c,\mathbf{K}+(m_c/M)\mathbf{q}}^\dagger c_{v,\mathbf{K}-(m_v/M)\mathbf{q}} |\Phi_0\rangle \quad (1.20)$$

$$E_n(\mathbf{q}) = \Delta + \frac{\hbar^2 q^2}{2M} - \frac{\mu e^4}{2c^2 \hbar^2} \frac{1}{n^2}, \quad (1.21)$$

with the coefficients $A_{\mathbf{q}}^n(\mathbf{K})$ obeying Eq. (1.15).

Note that the exciton energies are found to be below the uncorrelated electron-hole energies (Fig. 1.2).

By defining the exciton creation operators

$$a_{\mathbf{q},n}^\dagger = \sum_{\mathbf{K}} A_{\mathbf{q}}^n(\mathbf{K}) c_{c,\mathbf{K}+(m_c/M)\mathbf{q}}^\dagger c_{v,\mathbf{K}-(m_v/M)\mathbf{q}} \quad (1.22)$$

these new states can be considered as quasiparticles. A calculation of the commutator

$$[a_{0,n}, a_{0,n}^\dagger] = \sum_{\mathbf{K}} |A_0^n(\mathbf{k})|^2 \left\{ 1 - c_{c,\mathbf{K}}^\dagger c_{c,\mathbf{K}} - c_{v,\mathbf{K}} c_{v,\mathbf{K}}^\dagger \right\}, \quad (1.23)$$

shows that these particles behave approximately as bosons and the deviation is proportional to the density of electrons in the conduction and holes in the valence band [12, 19], where for simplicity we conducted the calculation for excitons of zero total momentum.

Thus it is clear that the Hamiltonian becomes diagonal in the basis of excitons

$$H = \sum_{\mathbf{q}, n} E_n(\mathbf{q}) a_{\mathbf{q}, n}^\dagger a_{\mathbf{q}, n}. \quad (1.24)$$

In the following discussion we will focus on the lowest internal state ($\Phi_n = \Phi_{1s}$) only and thus drop the index n .

1.2 Polariton Theory

As mentioned earlier polaritons arise from the interaction of excitons with photons. So in order to describe the polariton modes we have to construct the full Hamiltonian of the exciton-photon system. This Hamiltonian consists of three parts, namely the exciton, the photon and the interaction Hamiltonian.

$$H = H_x + H_{em} + H_I \quad (1.25)$$

Let's first consider the Hamiltonian without interaction

$$H_0 = H_x + H_{em}. \quad (1.26)$$

We have seen in the previous section that excitons are (in the low excitation limit) bosonic quasiparticles with a quadratic dispersion

$$E_x(\mathbf{k}) = \hbar\omega_x(\mathbf{k}) = E_0 + \frac{\hbar^2 k^2}{2M}. \quad (1.27)$$

Thus the second quantized form of the exciton Hamiltonian is

$$H_x = \sum_{\mathbf{k}} \hbar\omega_x(\mathbf{k}) a_{\mathbf{k}}^\dagger a_{\mathbf{k}}. \quad (1.28)$$

The photon Hamiltonian has the well known second quantized form [11]

$$H_{em} = \sum_{\mathbf{k}} \frac{\hbar c}{n_r} |\mathbf{k}| A_{\mathbf{k}}^{\dagger} A_{\mathbf{k}}, \quad (1.29)$$

where $A_{\mathbf{k}}^{\dagger}$ and $A_{\mathbf{k}}$ are the bosonic creation and annihilation operators for photons and n_r is the refraction index of the semiconductor material. We neglected the polarisation index, as for the moment we are only interested in a qualitative description. Obviously the natural basis of H_0 consists of the direct product states of exciton and photon Fock states and consequently an eigenvector can be written as

$$\left| n_{\mathbf{k}_1}^x, n_{\mathbf{k}_2}^x, n_{\mathbf{k}_3}^x, \dots \right\rangle \otimes \left| n_{\mathbf{k}_1}^{ph}, n_{\mathbf{k}_2}^{ph}, n_{\mathbf{k}_3}^{ph}, \dots \right\rangle, \quad (1.30)$$

where the quantities $n_{\mathbf{k}}^x$ and $n_{\mathbf{k}}^{ph}$ stand for the exciton and photon occupation numbers in the state \mathbf{k} , respectively.

In the next step we are going to introduce the exciton-photon interaction. It is crucial to realize where this interaction has its origin in. The exciton is, as we have seen earlier, an excitation of the whole electron many body system and with that in mind it is clear that the exciton-photon coupling arises from the Coulomb interaction of every single electron with the radiation field.

The Hamiltonian for electrons interacting with light can be written using the canonical momentum [31] and reads in first quantisation

$$H = \sum_i \frac{1}{2m_0} (\mathbf{p}_i - e\mathbf{A}(\mathbf{r}_i))^2, \quad (1.31)$$

where $\mathbf{A}(\mathbf{r}_i) = \sum_{\mathbf{k}} A_{0,\mathbf{k}} \left\{ A_{\mathbf{k}}^{\dagger} \epsilon_{\mathbf{k}} e^{-i\mathbf{k}\mathbf{r}_i} + h.c. \right\}$ is the electromagnetic vector potential and e and m_0 are the electron charge and mass, respectively. Moreover, \mathbf{r}_i and \mathbf{p}_i are the position and momentum of the i th electron. In the Coulomb gauge the vector potential commutes with the electron momentum $[\mathbf{A}(\mathbf{r}_i), \mathbf{p}_i] = 0$, since $\nabla \cdot \mathbf{A} = 0$. Therefore, by expanding the square in Eq. 1.31 we obtain

$$H = \sum_i \left\{ \frac{\mathbf{p}_i^2}{2m_0} - \frac{e}{m_0} \mathbf{A}(\mathbf{r}_i) \cdot \mathbf{p}_i + \frac{e^2}{2m_0} \mathbf{A}^2(\mathbf{r}_i) \right\}. \quad (1.32)$$

The first term in the latter equation is part of the exciton Hamiltonian H_x and so we identify the interaction Hamiltonian as

$$H_I = -\frac{e}{m_0} \sum_i \mathbf{A}(\mathbf{r}_i) \cdot \mathbf{p}_i + \frac{e^2}{2m_0} \sum_i \mathbf{A}^2(\mathbf{r}_i). \quad (1.33)$$

Note that the summation in Eq. (1.33) runs over all the electrons of the system. It is not straightforward to find the second quantized form of that operator, as one has to perform the transition from electron to exciton operators [41]. After a somewhat lengthy calculation the result is

$$H_I = i \sum_{\mathbf{k}} g_{\mathbf{k}} \left(A_{\mathbf{k}}^\dagger + A_{-\mathbf{k}} \right) \left(a_{\mathbf{k}} - a_{-\mathbf{k}}^\dagger \right) + \sum_{\mathbf{k}} d_{\mathbf{k}} \left(A_{\mathbf{k}}^\dagger + A_{-\mathbf{k}} \right) \left(A_{\mathbf{k}}^\dagger + A_{-\mathbf{k}} \right), \quad (1.34)$$

with the constants

$$g_{\mathbf{k}} = \omega_x(k) \sqrt{\frac{2\pi\hbar}{ckV}} \left\langle \Psi(\mathbf{k}) \left| \epsilon \mathbf{r} e^{i\mathbf{k}\mathbf{r}} \right| \Phi_0 \right\rangle \quad (1.35)$$

$$d_{\mathbf{k}} = \omega_x(k) \frac{2\pi}{ckV} \left| \left\langle \Psi(\mathbf{k}) \left| \epsilon \mathbf{r} e^{i\mathbf{k}\mathbf{r}} \right| \Phi_0 \right\rangle \right|^2. \quad (1.36)$$

The first part in Eq. (1.34) originates from the $\mathbf{A} \cdot \mathbf{p}$ -term, whereas the second part arises from the \mathbf{A}^2 -term. ϵ is the polarisation vector of the electromagnetic field, which will be discussed later.

Putting Eqs. (1.28), (1.29) and (1.34) together we realize that the full Hamiltonian is separable in \mathbf{k} .

$$H = \sum_{\mathbf{k}} h(\mathbf{k}) \quad (1.37)$$

For each \mathbf{k} and $-\mathbf{k}$ pair we have an equation that describes a system of four coupled harmonic oscillators $\{A_{\mathbf{k}}, A_{-\mathbf{k}}, a_{\mathbf{k}}, a_{-\mathbf{k}}\}$. Hopfield presented a scheme to diagonalize this Hamiltonian exactly by introducing suitable operational transformations [20]

$$\begin{pmatrix} \alpha_{\mathbf{k}}^1 \\ \alpha_{\mathbf{k}}^2 \\ \alpha_{-\mathbf{k}}^1 \\ \alpha_{-\mathbf{k}}^2 \end{pmatrix} = \begin{pmatrix} C_{11} & C_{12} & C_{13} & C_{14} \\ C_{21} & C_{22} & C_{23} & C_{24} \\ C_{31} & C_{32} & C_{33} & C_{34} \\ C_{41} & C_{42} & C_{43} & C_{44} \end{pmatrix} \cdot \begin{pmatrix} A_{\mathbf{k}} \\ a_{\mathbf{k}} \\ A_{-\mathbf{k}} \\ a_{-\mathbf{k}} \end{pmatrix}. \quad (1.38)$$

$\alpha_{\mathbf{k}}^1$ and $\alpha_{\mathbf{k}}^2$ are the polariton operators for the upper and lower polariton mode, respectively. By replacing the former operators by the polariton creation and annihilation operators and introducing a corresponding basis the polariton Hamiltonian $H_P = H_x + H_{em} + H_I$ is diagonal in terms of the new operators and has the form

$$H_P = \sum_{\xi=1,2} \sum_{\mathbf{k}} E_P^\xi(\mathbf{k}) \alpha_{\mathbf{k}}^{\xi\dagger} \alpha_{\mathbf{k}}^\xi. \quad (1.39)$$

In general, the coefficients C_{ij} of the Hopfield transformation in Eq. (1.38) have the complicated form given in [20]. But if we apply the rotating wave approximation and additionally drop the terms quadratic in the photon operator A (which is a good approximation in the low intensity limit [11]), the polariton operators are found to be

$$\alpha_{\mathbf{k}}^\xi = u_{\mathbf{k}}^\xi a_{\mathbf{k}} + v_{\mathbf{k}}^\xi A_{\mathbf{k}}, \quad (1.40)$$

where

$$u_{\mathbf{k}}^\xi = \sqrt{\frac{\Omega_{\mathbf{k}}^\xi - \omega_{ph}(\mathbf{k})}{2\Omega_{\mathbf{k}}^\xi - \omega_{ph}(\mathbf{k}) - \omega_x(\mathbf{k})}} \quad (1.41)$$

$$v_{\mathbf{k}}^\xi = \pm i \sqrt{\frac{\Omega_{\mathbf{k}}^\xi - \omega_x(\mathbf{k})}{2\Omega_{\mathbf{k}}^\xi - \omega_{ph}(\mathbf{k}) - \omega_x(\mathbf{k})}} \quad (1.42)$$

$$\Omega_{\mathbf{k}}^\xi = \frac{1}{2}(\omega_x(\mathbf{k}) + \omega_{ph}(\mathbf{k})) \pm \frac{1}{2}\sqrt{(\omega_x(\mathbf{k}) - \omega_{ph}(\mathbf{k}))^2 + (2g_{\mathbf{k}})^2}. \quad (1.43)$$

In the latter equations, the + and - signs correspond to the upper ($\xi = 1$) and lower ($\xi = 2$) polariton modes respectively. Note that in the limit $(\omega_x - \omega_{ph})^2 \gg (2g)^2$ we regain the unaltered exciton and photon modes.

A plot of the Polariton energies $E_P^1(\mathbf{k})$ and $E_P^2(\mathbf{k})$ shows the anticrossing behaviour of the polariton modes at resonance (Fig. 1.3). In Fig. 1.4 the exciton and photon shares of the upper polariton are depicted.

In the limits $k \rightarrow 0$ and $k \rightarrow \infty$ the upper polariton becomes purely excitonic and photonic, respectively. At resonance however, the polariton consist of an excitonic and a photonic part of equal weight.

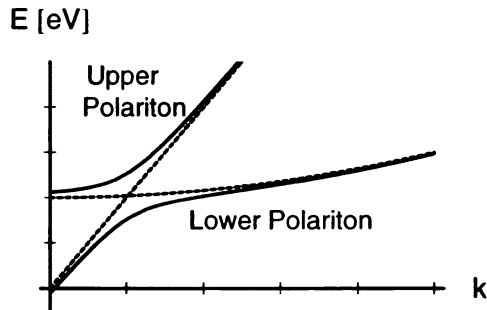


Figure 1.3. The Polariton dispersion. The dashed lines are the exciton and photon dispersions without interaction. Note that this sketch is not to scale.

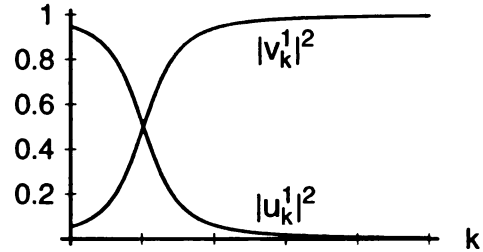


Figure 1.4. The exciton and photon shares, $u_{\mathbf{k}}^1$ and $v_{\mathbf{k}}^1$ of the upper polariton mode

1.3 Confined Excitons

Up to now we only considered excitons in a bulk material. In order to describe excitons in low dimensional quantum structures we have to find a way to confine both conduction electrons and holes in the same region. With that in mind it is plausible that conventional confinement potentials like e.g. in electric or magnetic traps are not applicable, as they act on conduction and valence electrons in the same way and consequently in an opposite manner on holes. In fact, a simple zeroth order calculation shows that an electron potential $V(\mathbf{r}_i)$ acts on holes like a potential $-V(\mathbf{r}_i)$. So it is obvious that it is impossible to confine both electrons and holes in the same region by applying a conventional potential.

The method to arrange such a confinement for electrons and holes is to make use of the band alignment of two different semiconductors. In this case a low dimensional semiconductor structure is embedded in a bulk semiconductor of a different type, with a conduction band structure like the one depicted in Fig. 1.5.

For the numerical calculations in Chapter 3 we will use a $GaAs/Al_{0.3}Ga_{0.7}As$ system, i.e. the $GaAs$ structure is embedded in $Al_{0.3}Ga_{0.7}As$.

Although an exact solution for this problem has not been presented in literature

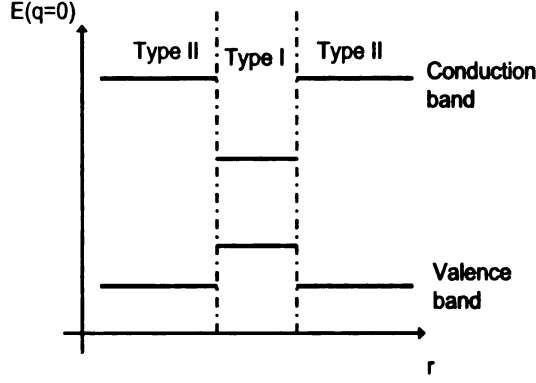


Figure 1.5. In zeroth order the bandstructure varies spatially like a step function at the edge of two semiconductors

so far, in the effective mass equation (1.18) this particular band structure is usually represented as an effective potential for both electrons and holes [34]. Thus, the effective mass Hamiltonian (1.18) for the electron hole system reads as [46]

$$\left(-\frac{\hbar^2}{2m_c} \nabla_{\mathbf{r}_e}^2 - \frac{\hbar^2}{2m_v} \nabla_{\mathbf{r}_h}^2 - \frac{e^2}{\epsilon |\mathbf{r}_e - \mathbf{r}_h|} + V_e(\mathbf{r}_e) + V_h(\mathbf{r}_h) \right) \Psi_x = \tilde{E} \Psi_x. \quad (1.44)$$

As our aim is to describe excitons in a nearly two dimensional structure, we assume the z-direction confinement potentials to be strong enough to confine the exciton in the x-y plane. Therefore the Coulomb potential only depends on the in-plane distance $\rho = \rho_e - \rho_h$. Moreover in case of a very strong confinement in z-direction the potentials approximately separate in the z and in-plane components as

$$V_e(\mathbf{r}_e) = V_e(\rho_e) + U_e(z_e), \quad (1.45)$$

as well as

$$V_h(\mathbf{r}_h) = V_h(\rho_h) + U_e(z_h). \quad (1.46)$$

This choice makes the Hamiltonian separable in z and ρ and the exciton wave function can be written as

$$\Psi_x(\mathbf{r}_e, \mathbf{r}_h) = \Phi(\rho_e, \rho_h) \phi_e(z_e) \phi_e(z_h), \quad (1.47)$$

with the notation $\mathbf{r}_{e/h} = (\rho_{e/h}, z_{e/h})$.

In case of a strong and narrow confinement it is plausible to assume a rectangular potential for both electrons and holes [7] and so the functions ϕ_e and ϕ_h are just the eigenfunction for a particle in a box. The remaining problem is to solve the in-plane Hamiltonian

$$\left(-\frac{\hbar^2}{2m_e} \nabla_{\rho_e}^2 - \frac{\hbar^2}{2m_h} \nabla_{\rho_h}^2 - \frac{e^2}{\epsilon |\rho|} + V_e(\rho_e) + V_h(\rho_h) \right) \Psi_x = \tilde{E} \Psi_x. \quad (1.48)$$

After introducing the center of mass coordinates

$$\rho = \rho_e - \rho_h \quad (1.49)$$

$$\mathbf{R} = \frac{m_e \rho_e + m_h \rho_h}{M}, \quad (1.50)$$

we expand the potentials in powers of ρ and find

$$\begin{aligned} V_e(\rho_e) &= V_e(\mathbf{R} + \frac{m_h}{M} \rho) = V_e(\mathbf{R}) + \nabla V_e(\mathbf{R}) \frac{m_h}{M} \rho + O(\rho^2) \\ &\approx V_e(\mathbf{R}) \end{aligned} \quad (1.51)$$

and

$$\begin{aligned} V_h(\rho_h) &= V_h(\mathbf{R} - \frac{m_e}{M} \rho) = V_h(\mathbf{R}) - \nabla V_h(\mathbf{R}) \frac{m_e}{M} \rho + O(\rho^2) \\ &\approx V_h(\mathbf{R}). \end{aligned} \quad (1.52)$$

Since the exciton Bohr radius is much smaller than the confinement radius (due to the strong Coulomb potential), we only have to keep the zeroth order in the latter expansion. In that limit the Hamiltonian separates in the relative and center-of-mass in-plane motion and finally the envelope function can be written as

$$\Psi_x(\mathbf{r}_e, \mathbf{r}_h) = \chi(\mathbf{R}) \Phi(\rho) \phi_e(z_e) \phi_h(z_h), \quad (1.53)$$

where $\Phi(\rho)$ is the solution of the two dimensional hydrogen-like problem

$$\left(-\frac{\hbar^2}{2\mu} \nabla_{\rho}^2 - \frac{e^2}{\epsilon |\rho|} \right) \Phi(\rho) = E_{rel} \Phi(\rho), \quad (1.54)$$

and $\chi(\mathbf{R})$ is the solution of the problem

$$\left(-\frac{\hbar^2}{2M}\nabla_{\mathbf{R}}^2 + V_e(\mathbf{R}) + V_h(\mathbf{R})\right)\chi(\mathbf{R}) = E_{cm}\chi(\mathbf{R}). \quad (1.55)$$

The eigenenergies of a bound 2D exciton state consequently are

$$E = \Delta + E_{ze} + E_{zh} + E_{cm} + E_{rel}, \quad (1.56)$$

where E_{ze} and E_{zh} are the quantized energies for an electron and a hole in a 1D box, respectively.

We should note that Kumar et al. [26] showed that the in-plane confining potential for both electrons and holes in a quantum dot (or the in-plane directions of a quantum disc) can be approximated reasonably well by a parabolic potential. This has the great advantage that the preceding approximations in Eqs. (1.51) and (1.52) are not necessary, as the relative and center-of-mass motion separate exactly. The latter then turns out to be harmonic oscillator like.

Like in the case of excitons in bulk material, we can define exciton creation and annihilation operators,

$$a_{\alpha}^{\dagger} = \sum_{\mathbf{k}, \mathbf{k}'} A_{\alpha}(\mathbf{k}, \mathbf{k}') c_{\mathbf{k}}^{\dagger} c_{\mathbf{k}'} \quad (1.57)$$

and

$$a_{\alpha} = \left(a_{\alpha}^{\dagger}\right)^{\dagger}. \quad (1.58)$$

Here, α denotes a set of quantum numbers, which characterize the state of the in-plane, center of mass as well as the electron and hole z-direction motion and $A_{\alpha}(\mathbf{k}, \mathbf{k}')$ is the Fourier transform of the exciton wave function in Eq. (1.53). The commutator

of this new defined operators is

$$\begin{aligned}
[a_\alpha, a_{\alpha'}^\dagger] &= \sum_{\mathbf{k}_1, \mathbf{k}_2, \mathbf{k}_3, \mathbf{k}_4} A_\alpha^*(\mathbf{k}_1, \mathbf{k}_2) A_{\alpha'}(\mathbf{k}_3, \mathbf{k}_4) [c_{v\mathbf{k}_2}^\dagger c_{c\mathbf{k}_1}, c_{c\mathbf{k}_3}^\dagger c_{v\mathbf{k}_4}] \\
&= \sum_{\mathbf{k}, \mathbf{k}'} A_\alpha^*(\mathbf{k}, \mathbf{k}') A_{\alpha'}(\mathbf{k}, \mathbf{k}') - \sum_{\mathbf{k}_1, \mathbf{k}_2, \mathbf{k}_4} A_\alpha^*(\mathbf{k}_1, \mathbf{k}_2) A_{\alpha'}(\mathbf{k}_1, \mathbf{k}_4) c_{v\mathbf{k}_4} c_{v\mathbf{k}_2}^\dagger \\
&\quad - \sum_{\mathbf{k}_1, \mathbf{k}_2, \mathbf{k}_3} A_\alpha^*(\mathbf{k}_1, \mathbf{k}_2) A_{\alpha'}(\mathbf{k}_3, \mathbf{k}_2) c_{c\mathbf{k}_3}^\dagger c_{c\mathbf{k}_1}. \tag{1.59}
\end{aligned}$$

The first term of the RHS gives a delta function due to the orthogonality of the eigenstates, so that we get

$$\begin{aligned}
[a_\alpha, a_{\alpha'}^\dagger] &= \delta_{\alpha, \alpha'} - \sum_{\mathbf{k}_1, \mathbf{k}_2, \mathbf{k}_4} A_\alpha^*(\mathbf{k}_1, \mathbf{k}_2) A_{\alpha'}(\mathbf{k}_1, \mathbf{k}_4) c_{v\mathbf{k}_4} c_{v\mathbf{k}_2}^\dagger \\
&\quad - \sum_{\mathbf{k}_1, \mathbf{k}_2, \mathbf{k}_3} A_\alpha^*(\mathbf{k}_1, \mathbf{k}_2) A_{\alpha'}(\mathbf{k}_3, \mathbf{k}_2) c_{c\mathbf{k}_3}^\dagger c_{c\mathbf{k}_1}. \tag{1.60}
\end{aligned}$$

In the limit of an infinite dot size we recover the relation (1.23) for the QW case which implies a bosonic behaviour if the exciton density is much smaller than a saturation density $n_{saturation} \approx 1/(2\pi a_B^2)$, where a_B denotes the two dimensional exciton Bohr radius [10, 9].

In contrast, in the limit of point-like dots excitons behave as fermions [50]. Being in an intermediate regime we have to be careful about making assertions concerning the behaviour of excitons on mesoscopic structures like the quantum dots we are considering. However, according to reference [50], the large in-plane size of the dots we are considering (approx. 50 nm compared to a the 2D exciton Bohr radius of GaAs of $a_B = 5.8$ nm) suggests that we can expect a bosonic behaviour.

CHAPTER 2

The Model

The system we are about to study consists of a periodic array of N identical semiconductor quantum dots embedded in a planar microcavity (Fig. 2.1). It is similar to the system examined in reference [49], where we replaced the quantum well by a quantum dot lattice.

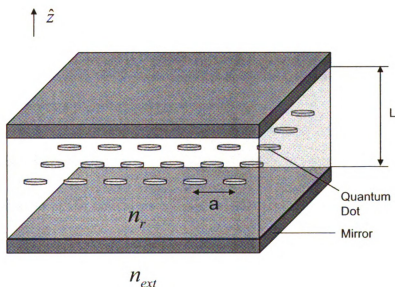


Figure 2.1. N identical quantum dots of disc-like shape in an ideal periodic array embedded in a planar microcavity.

The dots are assumed to have a cylindrical, disc-like shape, like the ones described in reference [46] (Fig. 2.2).

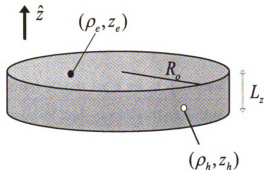


Figure 2.2. The quantum dots we are considering have a cylindrical, disc-like shape. The thickness of the dot is labelled by L_z and the radius by R_0 .

We are going to study the interaction of the confined electromagnetic field with the QD excitons.

Unlike in the quantum well case, the exciton-photon interaction does not conserve the in-plane momentum, if the exciton is confined to a quantum dot structure. This prevents obtaining an exact solution to the problem [47]. As we will see, the spacial periodicity of our system restores a quasi-momentum conservation. This feature allows us to diagonalize the system hamiltonian with a few approximations and to analyse the resulting polariton energy dispersions.

2.1 The Hamiltonian

The Hamiltonian of the system we consider consists of three terms:

$$H = H_x + H_{em} + H_{int}. \quad (2.1)$$

In the following we introduce each term separately before analysing the full Hamiltonian.

2.1.1 The Exciton Hamiltonian

The first term we are going to discuss is the exciton Hamiltonian, H_x .

Within the quasiparticle picture introduced in the previous chapter, a quantum dot

exciton can be in bound states with discrete energies

$$E_\alpha = \Delta + E_{ze}^{\alpha_1} + E_{zh}^{\alpha_2} + E_{cm}^{\alpha_3} + E_{rel}^{\alpha_4}, \quad (2.2)$$

where $\alpha = (\alpha_1, \alpha_2, \alpha_3, \alpha_4)$ stands for a set of quantum numbers characterizing the state of the in-plane, center-of-mass as well as the electron and hole z-direction motion.

The corresponding eigenfunctions are indicated by

$$|\Psi_x^\alpha\rangle = a_\alpha^\dagger |\Phi_0\rangle. \quad (2.3)$$

As we cannot expect an exact bosonic behaviour of the exciton operators we limit ourselves to the case of a single exciton. Thus, in second quantisation we find the Hamiltonian to be

$$H_x(1) = \sum_{\alpha} E_\alpha a_\alpha^\dagger a_\alpha. \quad (2.4)$$

For simplicity, we will only include the ground state and the first excited state in the calculations and we thus drop the index α .

Instead of a single dot we consider a system of N dots arranged in a periodic lattice. If the separation between the dots is large enough (large enough that the center-of-mass wave functions of excitons on two different dots have no significant overlap) we can treat each dot separately. Besides, we assume the dots to be identical, so that we find the same effective potential for electrons (and for holes) on every dot. This implies that the effective potential on the i th dot can be written as

$$V_e^i(\mathbf{R}) = V_e^0(\mathbf{R} - \mathbf{R}_i) \quad (2.5)$$

for electrons and

$$V_h^i(\mathbf{R}) = V_h^0(\mathbf{R} - \mathbf{R}_i) \quad (2.6)$$

for holes, where \mathbf{R}_i identifies the center of the i th dot (index 0 indicates the dot at the origin). It is obvious that this property of the potentials implies for the related center of mass wave functions

$$\chi_i(\mathbf{R}) = \chi_0(\mathbf{R} - \mathbf{R}_i). \quad (2.7)$$

Consequently the wave function for an exciton on the i th dot reads

$$\Psi_x^i(\mathbf{r}_e, \mathbf{r}_h) = \chi_0(\mathbf{R} - \mathbf{R}_i)\Phi(\rho)\phi_e(z_e)\phi_e(z_h), \quad (2.8)$$

and we can write the Hamiltonian for the quantum dot array as a sum over the Hamiltonians from the N sites.

$$H_x = \sum_{i=1}^N H_x(i) = \sum_i \hbar\omega_x a_i^\dagger a_i, \quad (2.9)$$

where the operator a_i^\dagger creates an exciton (in the lowest excited state) on the dot i .

Consequently the eigenstates of the system can be written as Fock states:

$$|n_1, n_2, \dots\rangle = \left(a_1^\dagger\right)^{n_1} \left(a_2^\dagger\right)^{n_2} \dots |\phi_0\rangle, \quad (2.10)$$

where we restrict the occupation number n_i , i.e. the number of excitons on dot i , to $\{0, 1\}$.

Note that we have set the ground state energy to zero.

According to our assumption that the exciton wave functions from different dots have no significant overlap, the operators $a_i^{(\dagger)}$ obey the commutation relations

$$[a_i, a_j^\dagger] = \delta_{i,j} [a, a^\dagger], \quad (2.11)$$

where the commutator $[a, a^\dagger]$ stands for the expression derived in Eq. (1.60) for $\alpha = \alpha' = 0$. In order to exploit the periodicity of our system we are going to introduce new operators

$$a_{\mathbf{q}}^\dagger := \frac{1}{\sqrt{N}} \sum_{i=1}^N a_i^\dagger e^{i\mathbf{q}\mathbf{R}_i} \quad (2.12)$$

and

$$a_{\mathbf{q}} := \left(a_{\mathbf{q}}^\dagger\right)^\dagger = \frac{1}{\sqrt{N}} \sum_{i=1}^N a_i e^{-i\mathbf{q}\mathbf{R}_i}. \quad (2.13)$$

These operators obey the same commutation relations as the localized operators

$$\begin{aligned} [a_{\mathbf{q}}, a_{\mathbf{q}'}^\dagger] &= \frac{1}{N} \sum_{i,j} e^{i\mathbf{q}\mathbf{R}_i} e^{-i\mathbf{q}'\mathbf{R}_j} \underbrace{[a_i, a_j^\dagger]}_{\delta_{i,j}[a, a^\dagger]} \\ &= \frac{1}{N} \sum_i e^{i(\mathbf{q}-\mathbf{q}')\mathbf{R}_i} [a, a^\dagger] = \delta_{\mathbf{q}, \mathbf{q}'} [a, a^\dagger]. \end{aligned} \quad (2.14)$$

Moreover, they reflect the periodicity of the lattice as for each reciprocal lattice vector \mathbf{Q} we have

$$a_{\mathbf{q}+\mathbf{Q}}^{(\dagger)} = \frac{1}{\sqrt{N}} \sum_{i=1}^N a_i^{(\dagger)} e^{\pm i\mathbf{q}\mathbf{R}_i} e^{\pm i\mathbf{Q}\mathbf{R}_i} = a_{\mathbf{q}}^{(\dagger)}, \quad (2.15)$$

since by definition of the reciprocal lattice it is $e^{i\mathbf{Q}\mathbf{R}_i} = 1$. So we see that the quantum number \mathbf{q} can be restricted to the first Brillouin zone and if we use periodic boundary conditions we find exactly N discrete, possible values for \mathbf{q} . Accordingly, the inverse expression for Eq. (2.12) is

$$a_i^\dagger := \frac{1}{\sqrt{N}} \sum_{\mathbf{q} \in 1.BZ} a_{\mathbf{q}}^\dagger e^{-i\mathbf{q}\mathbf{R}_i}. \quad (2.16)$$

We would like to express the exciton Hamiltonian, H_x , in terms of these new operators and thus we insert the latter expression in Eq. (2.9). By exploiting the useful property

$$\sum_i e^{i(\mathbf{q}-\mathbf{q}')\mathbf{R}_i} = N\delta_{\mathbf{q},\mathbf{q}'} \quad (2.17)$$

we obtain

$$H_x = \hbar\omega_x \sum_{\mathbf{q} \in 1.BZ} a_{\mathbf{q}}^\dagger a_{\mathbf{q}}. \quad (2.18)$$

This implies that the excitons in our model are quasiparticles with a quantized in-plane momentum \mathbf{q} , restricted to the first Brillouin zone, and an infinite mass. Furthermore, we have seen that these quasiparticles obey the same commutation relations as the QD excitons in Section 1.3.

The natural basis for this Hamiltonian is

$$|n_{\mathbf{q}_1}, n_{\mathbf{q}_2}, \dots\rangle = \left(a_{\mathbf{q}_1}^\dagger\right)^{n_{\mathbf{q}_1}} \left(a_{\mathbf{q}_2}^\dagger\right)^{n_{\mathbf{q}_2}} \dots |\phi_0\rangle, \quad (2.19)$$

where $n_{\mathbf{q}_i}$ is a counter for excitons in the state $a_{\mathbf{q}_i}^\dagger |\Phi_0\rangle$, restricted to $\{0, 1\}$.

Please note that we changed our single particle basis from a set of completely localized states $a_i^\dagger |\Phi_0\rangle$ to a set of completely delocalized states $a_{\mathbf{q}}^\dagger |\Phi_0\rangle$.

2.1.2 The Photon Hamiltonian

In this section we are going to provide a quantum mechanical description of electromagnetic radiation inside a semiconductor microcavity. A microcavity is basically a device to confine the electromagnetic field. The simplest structure for such a confinement is a planar Fabry-Pérot resonator.

This structure consists of two parallel mirrors of a high reflectivity separated by a dielectric material called the 'spacer'. Classically, an electromagnetic field can only exist between the mirrors, if the successive passes of a propagating wave interfere constructively. This leads to the condition that the wave vector perpendicular to the mirrors k_z has to obey the condition

$$k_z L = n\pi, \quad (2.20)$$

where $n = 1, 2, 3 \dots$ or

$$L \sqrt{\frac{\omega^2}{c^2} n_r^2 - \mathbf{k}_{\parallel}^2} = n\pi, \quad (2.21)$$

where ω is the photon frequency, \mathbf{k}_{\parallel} is the component of the photon wave vector parallel to the mirrors, L is the cavity spacing and n_r is the refraction index of the dielectric spacer. The latter equation tells us that the main effect of a microcavity is the quantization of the electromagnetic field in the direction of the confinement; in our case the z -direction.

The second quantization form of the electromagnetic field inside a microcavity is obtained using the standard procedure of replacing the amplitudes of the vector potential in its expansion into plane waves by photon creation and annihilation operators [11]. Because of the special symmetry of the microcavity, it turns out to be convenient to define certain photon polarizations, which we call E-mode ($E_z = 0$) and M-mode ($B_z = 0$). The definition of these modes is in analogy with the TE and TM modes of a waveguide [23]. The field operators for the E- and M-modes can be

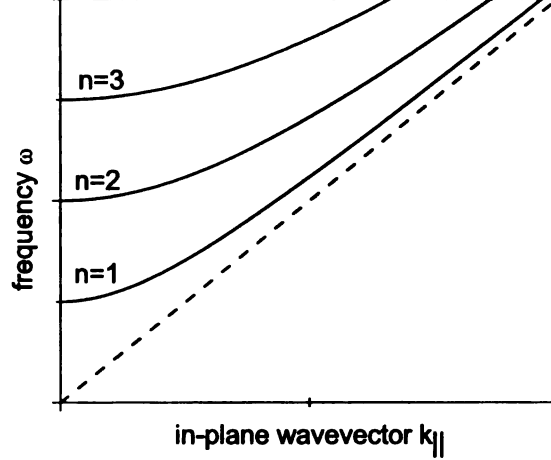


Figure 2.3. The in-plane dispersion modes ($n=1,2,3$) of a microcavity. The dashed line is the two dimensional dispersion of a free photon.

written as [4]

$$\mathbf{A}_{\mathbf{k}E}(\mathbf{r}) = \sqrt{\frac{\hbar}{\epsilon_0 n_T^2 \omega_{\mathbf{k}} V}} \cos(k_z z) \hat{q} \times \hat{z} e^{i\mathbf{q}\rho} \hat{A}_{\mathbf{k}E} + h.c. \quad (2.22)$$

$$\mathbf{A}_{\mathbf{k}M}(\mathbf{r}) = \sqrt{\frac{\hbar}{\epsilon_0 n_T^2 \omega_{\mathbf{k}} V}} \left(-\frac{q}{k} \sin(k_z z) \hat{z} - i \frac{k_z}{k} \cos(k_z z) \hat{q} \right) e^{i\mathbf{q}\rho} \hat{A}_{\mathbf{k}M} + h.c., \quad (2.23)$$

where $\hat{A}_{\mathbf{k}E}$ and $\hat{A}_{\mathbf{k}M}$ are the destruction operators for photons in the E- and M-mode, respectively. As usual the notation is $\mathbf{k} = (\mathbf{q}, k_z)$ as well as $\mathbf{r} = (\rho, z)$. V is an arbitrary quantisation volume, which we choose to be identical to the quantisation volume that appeared in the treatment of QD lattice excitons in the previous section.

The operators $\hat{A}_{\mathbf{k}E}$ and $\hat{A}_{\mathbf{k}M}$ are normalized, so that energy of the field is $\hbar\omega_{\mathbf{k}}(n + 1/2)$ when there are n photons in the corresponding mode. Consequently, the photon Hamiltonian can be written in the form

$$H_{em} = \sum_{k_z} \sum_{\mathbf{q}\nu} \hbar\omega_{\mathbf{k}} \hat{A}_{\mathbf{k}\nu}^\dagger \hat{A}_{\mathbf{k}\nu}. \quad (2.24)$$

Since we will tune the cavity spacing in a way that the exciton energy matches the energy of the first cavity mode ($k_z = \pi/L$) we can neglect the rest of the modes as

they are off-resonant. Therefore the Hamiltonian simplifies to

$$H_{em} = \sum_{\mathbf{q}\nu} \hbar\omega_{\mathbf{k}} \hat{A}_{\mathbf{k}\nu}^\dagger \hat{A}_{\mathbf{k}\nu}, \quad (2.25)$$

with $\mathbf{k} = (\mathbf{q}, \pi/L)$ and $\nu = E, M$.

2.1.3 Exciton-Photon Interaction

In this section we derive the interaction between the exciton on a quantum dot lattice and cavity photons from first principles.

At first we have to describe the coupling of one quantum dot at \mathbf{R}_j with the radiation field. As we have seen in Section 1.2 the exciton-photon interaction has to be expressed in terms of the electron-photon Hamiltonian in first quantisation (Eq. (1.33))

$$H_I(\mathbf{R}_j) = -\frac{e}{m_0} \sum_i \mathbf{A}(\mathbf{r}_i) \cdot \mathbf{p}_i + \frac{e^2}{2m_0} \sum_i \mathbf{A}^2(\mathbf{r}_i),$$

where the sum runs over all electrons in the dot at \mathbf{R}_j and m_0 denotes the electron mass. For low-intensity radiation the term quadratic in A becomes negligible [11]. This allows us to retain the linear term only and we can write the interaction as

$$H_I(\mathbf{R}_j) = -\frac{e}{m_0} \sum_i \mathbf{A}(\mathbf{r}_i) \cdot \mathbf{p}_i. \quad (2.26)$$

We have seen earlier that the exciton states $|\Psi_x^\alpha\rangle = a_\alpha^\dagger |\Phi_0\rangle$ form a complete set of basis vectors for the many body system in the quantum dot j . Therefore the completeness relation

$$\sum_\alpha |\Psi_x^\alpha\rangle \langle \Psi_x^\alpha| = I \quad (2.27)$$

holds and we can express the interaction in terms of the exciton functions by inserting the unity operator twice as

$$H_I(\mathbf{R}_j) = \frac{e}{m_0} \sum_{\alpha,\beta} |\Psi_x^\alpha\rangle \langle \Psi_x^\alpha| \sum_i \mathbf{A}(\mathbf{r}_i) \cdot \mathbf{p}_i |\Psi_x^\beta\rangle \langle \Psi_x^\beta|. \quad (2.28)$$

Using $\mathbf{p}_i = i\frac{m_0}{\hbar} [H_x(j), \mathbf{r}_i]$ and the fact that $H_x(j) |\Psi_x^\alpha\rangle = E_\alpha |\Psi_x^\alpha\rangle$ we can simplify the preceding equation to

$$H_I(\mathbf{R}_j) = i\frac{e}{\hbar} \sum_{\alpha,\beta} (E_\alpha - E_\beta) \langle \Psi_x^\alpha | \sum_i \mathbf{A}(\mathbf{r}_i) \cdot \mathbf{r}_i | \Psi_x^\beta \rangle | \Psi_x^\alpha \rangle \langle \Psi_x^\beta |. \quad (2.29)$$

As we did before we limit our single exciton basis to the lowest two states, i.e. the ground state $|\Phi_0\rangle$ and the first excited state, which we indicate by $|\Psi_x\rangle$. Before we proceed, we need to express the many electron operator $\sum_i \mathbf{A}(\mathbf{r}_i) \cdot \mathbf{r}_i$ in terms of a delocalized basis of Bloch functions (Eq. (1.3)). According to the second quantisation formalism this expansion is given by

$$\sum_i \mathbf{A}(\mathbf{r}_i) \mathbf{r}_i = \sum_{\substack{\mathbf{k}, \mathbf{k}' \\ \sigma, \sigma'}} t_{\mathbf{k}, \mathbf{k}'} c_{\mathbf{k}, \sigma}^\dagger c_{\mathbf{k}', \sigma'}, \quad (2.30)$$

where t stands for the matrix element

$$t_{\substack{\mathbf{k}, \mathbf{k}' \\ \sigma, \sigma'}} = \langle \mathbf{k}\sigma | \mathbf{A}(\mathbf{r}) \mathbf{r} | \mathbf{k}'\sigma' \rangle. \quad (2.31)$$

Using Eq.(1.57) it is straightforward to verify that Eq. (2.29) can be simplified to

$$H_I(\mathbf{R}_j) = ie\omega_x \left\{ \sum_{\mathbf{k}\mathbf{k}'} t_{\mathbf{k}, \mathbf{k}'} A^*(\mathbf{k}, \mathbf{k}') a_j^\dagger - \sum_{\mathbf{k}\mathbf{k}'} t_{\mathbf{k}', \mathbf{k}} A(\mathbf{k}, \mathbf{k}') a_j \right\}, \quad (2.32)$$

where we again used the orthogonality of the states $c_{\mathbf{k}, \sigma}^\dagger c_{\mathbf{k}', \sigma'} |\Phi_0\rangle$ and identified the expression $|\Psi_x\rangle \langle \Phi_0|$ with the creation operator a_j^\dagger and consequently the expression $|\Phi_0\rangle \langle \Psi_x|$ with the lowering operator a_j . Note that in Eq.(2.32) $A(\mathbf{k}, \mathbf{k}')$ indicates the Fourier transform of the exciton wave function as defined in Section 1.3 and should not be confused with the electromagnetic field in Eqs. (2.22) & (2.23).

At this point it is important to notice that the matrix element t is a completely delocalized quantity. The information that we are dealing with an exciton localized on a disc at position \mathbf{R}_j is entirely encoded in the coefficients $A(\mathbf{k}, \mathbf{k}')$. Note also that the values of \mathbf{k} and \mathbf{k}' are restricted to the first Brillouin zone.

Due to the property

$$\sum_{\mathbf{k}\mathbf{k}'} t_{\mathbf{k}',\mathbf{k}}^{v,c} A(\mathbf{k}, \mathbf{k}') = \left(\sum_{\mathbf{k}\mathbf{k}'} t_{\mathbf{k},\mathbf{k}'}^{c,v} A^*(\mathbf{k}, \mathbf{k}') \right)^\dagger, \quad (2.33)$$

the only thing that remains to be done is to evaluate the expression

$$\sum_{\mathbf{k}\mathbf{k}'} t_{\mathbf{k}',\mathbf{k}}^{v,c} A(\mathbf{k}, \mathbf{k}'). \quad (2.34)$$

After a somewhat lengthy calculation, which we present in Appendix B, the final result for the interaction Hamiltonian for one dot is:

$$H_I(\mathbf{R}_j) = \hbar \sum_{\mathbf{q}\sigma} \left\{ \tilde{g}_{\mathbf{k}}^{\sigma*}(\mathbf{R}_j) A_{\mathbf{k}\sigma} a_j^\dagger + \tilde{g}_{\mathbf{k}}^\sigma(\mathbf{R}_j) A_{\mathbf{k}\sigma}^\dagger a_j \right\}, \quad (2.35)$$

where \mathbf{q} denotes the in-plane component of the wave vector $\mathbf{k} = (\mathbf{q}, k_z)$ and the coupling constant is defined as

$$\tilde{g}_{\mathbf{k}}^E(\mathbf{R}_j) = ie\omega_x \Phi_{1s}(0) \frac{1}{\hbar} C_{\mathbf{k}} \tilde{\chi}_j(\mathbf{q}) I(k_z) u_{cv}, \quad (2.36)$$

for the E-mode. The coupling constant for the M-mode obeys the relation:

$$\tilde{g}_{\mathbf{k}}^M(\mathbf{R}_j) = -i \frac{k_z}{k} \tilde{g}_{\mathbf{k}}^E(\mathbf{R}_j). \quad (2.37)$$

The quantities in Eq. (2.36) are defined as

$$C_{\mathbf{k}} = \sqrt{\frac{\hbar}{\epsilon_0 n_r^2 \omega_{\mathbf{k}} V}} \quad (2.38)$$

$$I(k_z) = \int dz \phi_e(z) \phi_h(z) \cos(k_z z) \quad (2.39)$$

$$\tilde{\chi}_j(\mathbf{q}) = \int d\rho \chi_j(\rho) e^{-i\mathbf{q}\rho}, \quad (2.40)$$

and u_{cv} is the length of the in-plane component of

$$\mathbf{u}_{cv} = \frac{1}{V_{UC}} \int_{UC} d\mathbf{r} \mathbf{u}_v^*(\mathbf{r}) \mathbf{r} u_c(\mathbf{r}). \quad (2.41)$$

The function Φ_{1s} is the hydrogenic ground state of the Hamiltonian in Eq. (1.54) and V_{UC} is the volume of the crystal elementary unit cell.

Earlier we have seen (Eq. (2.8)) that the functions describing the center-of-mass motion for an exciton at site \mathbf{R}_j is related to that of an exciton at the origin by the equation

$$\chi_j(\rho) = \chi_0(\rho - \mathbf{R}_j). \quad (2.42)$$

In the lowest order approximation the center-of-mass potential is parabolic and the solution of Eq. (1.55) is a Gaussian of the form

$$\chi_0(\rho) = \frac{1}{\pi\beta} e^{-\frac{\rho^2}{\beta^2}}. \quad (2.43)$$

From here it is straightforward to derive that the Fourier transform of $\chi_j(\rho)$ reads

$$\tilde{\chi}_j(\mathbf{q}) = e^{-i\mathbf{q}\mathbf{R}_j} \tilde{\chi}_0(\mathbf{q}) = e^{-i\mathbf{q}\mathbf{R}_j} \sqrt{2\pi\beta} e^{-\frac{1}{4}\mathbf{q}^2\beta^2}, \quad (2.44)$$

which leads to the final form of the coupling constant

$$\tilde{g}_{\mathbf{k}}^E(\mathbf{R}_j) = i e^{-i\mathbf{q}\mathbf{R}_j} \frac{e}{\hbar} \omega_x \sqrt{N} \Phi_{1s}(0) C_{\mathbf{k}} \tilde{\chi}_0(\mathbf{q}) I(\pi/L) u_{cv}. \quad (2.45)$$

Because of our assumption of a negligible overlap for the exciton wave function at different sites the interaction Hamiltonian for the whole system is simply the sum of the terms for the N single dots

$$\begin{aligned} H_I &= \sum_j H_I(\mathbf{R}_j) \\ &= \hbar \sum_{\mathbf{q}\sigma} \left\{ g_{\mathbf{k}}^{\sigma*} A_{\mathbf{k}\sigma} \left(\frac{1}{\sqrt{N}} \sum_j a_j^\dagger e^{i\mathbf{q}\mathbf{R}_j} \right) + g_{\mathbf{k}}^\sigma A_{\mathbf{k}\sigma}^\dagger \left(\frac{1}{\sqrt{N}} \sum_j a_j e^{-i\mathbf{q}\mathbf{R}_j} \right) \right\} \\ &= \hbar \sum_{\mathbf{q}\sigma} \left\{ g_{\mathbf{k}}^{\sigma*} A_{\mathbf{k}\sigma} a_{\mathbf{q}}^\dagger + g_{\mathbf{k}}^\sigma A_{\mathbf{k}\sigma}^\dagger a_{\mathbf{q}} \right\}. \end{aligned} \quad (2.46)$$

where the constant $g_{\mathbf{k}}^E$ is defined as

$$\begin{aligned} g_{\mathbf{k}}^E &= \sqrt{N} \tilde{g}_{\mathbf{k}}^E(\mathbf{R} = 0) = i \frac{e}{\hbar} \omega_x \sqrt{N} \Phi_{1s}(0) C_{\mathbf{k}} \tilde{\chi}_0(\mathbf{q}) I(\pi/L) u_{cv} \\ &= i \sqrt{n} e \omega_x \sqrt{\frac{2\pi}{\hbar c_0 n_r^2}} \frac{1}{\sqrt{\omega_{\mathbf{k}}}} \frac{\beta}{\sqrt{L}} e^{-\frac{1}{4}\mathbf{q}^2\beta^2} \Phi_{1s}(0) I(\pi/L) u_{cv}, \end{aligned} \quad (2.47)$$

where $n = \frac{N}{S}$ stands for the number of dots per unit area. Moreover it is

$$g_{\mathbf{k}}^M = -i \frac{k_z}{k} g_{\mathbf{k}}^E. \quad (2.48)$$

Note that in Eq. (2.46) \mathbf{q} runs over the full reciprocal space. Therefore each vector \mathbf{q} in the sum can be expressed as a sum of a reciprocal lattice vector \mathbf{Q} and a vector within the first Brillouin zone \mathbf{q}' as

$$\mathbf{q} = \mathbf{Q} + \mathbf{q}'. \quad (2.49)$$

If we in addition take into account the periodicity of $a_{\mathbf{q}}$ given in Eq. (2.15) we can rewrite Eq. (2.46) as

$$H_I = \hbar \sum_{\mathbf{q}' \in 1.BZ} \sum_{\mathbf{Q} \in RL} \sum_{\sigma=E,M} \left\{ g_{\mathbf{q}'+\mathbf{Q}}^{\sigma*} A_{\mathbf{q}'+\mathbf{Q},\sigma} a_{\mathbf{q}'}^\dagger + g_{\mathbf{q}'+\mathbf{Q}}^\sigma A_{\mathbf{q}'+\mathbf{Q},\sigma}^\dagger a_{\mathbf{q}'} \right\}, \quad (2.50)$$

where the notation $A_{\mathbf{q}'+\mathbf{Q},\sigma}^\dagger \equiv A_{\mathbf{k}=(\mathbf{q}'+\mathbf{Q},\pi/L),\sigma}^\dagger$ as well as $g_{\mathbf{q}'+\mathbf{Q}}^\sigma \equiv g_{\mathbf{k}=(\mathbf{q}'+\mathbf{Q},\pi/L)}^\sigma$ is understood. Hence, the interaction Hamiltonian is separable in \mathbf{q}' .

2.2 Analysis of the full Hamiltonian

By combining Eqs. (2.18), (2.25) & (2.50) we compose the full Hamiltonian of the system. It can be separated in the variable \mathbf{q} , which is restricted to the first Brillouin zone of the two dimensional lattice of quantum dots.

$$H = \sum_{\mathbf{q} \in 1.BZ} h(\mathbf{q}), \quad (2.51)$$

where

$$\begin{aligned} h(\mathbf{q}) = & \hbar \omega_x a_{\mathbf{q}}^\dagger a_{\mathbf{q}} + \hbar \sum_{\sigma=E,M} \sum_{\mathbf{Q} \in RL} \omega_{\mathbf{q}+\mathbf{Q}} A_{\mathbf{q}+\mathbf{Q},\sigma}^\dagger A_{\mathbf{q}+\mathbf{Q},\sigma} \\ & + \hbar \sum_{\sigma=E,M} \sum_{\mathbf{Q} \in RL} \left\{ g_{\mathbf{q}+\mathbf{Q}}^{\sigma*} A_{\mathbf{q}+\mathbf{Q},\sigma} a_{\mathbf{q}}^\dagger + g_{\mathbf{q}+\mathbf{Q}}^\sigma A_{\mathbf{q}+\mathbf{Q},\sigma}^\dagger a_{\mathbf{q}} \right\}. \end{aligned} \quad (2.52)$$

In this form of the Hamiltonian the first remarkable feature of the system becomes manifest. Unlike in the case of one quantum dot, where the exciton couples to a bath of photon modes, or the opposite case of a quantum well, where there is a one to one correspondence in the exciton-photon coupling, in our system an exciton state $|\mathbf{q}\rangle = a_{\mathbf{q}}^\dagger |0\rangle$ couples to a discrete and yet infinite set of so called umklapp photon states $|\mathbf{1}_{\mathbf{q}+\mathbf{Q},\sigma}\rangle = A_{\mathbf{q}+\mathbf{Q},\sigma}^\dagger |0\rangle$, where \mathbf{Q} denotes a reciprocal lattice vector (Fig. 2.4). Similar umklapp photon processes and their role in polariton properties have been studied exhaustively in molecular crystals [8].

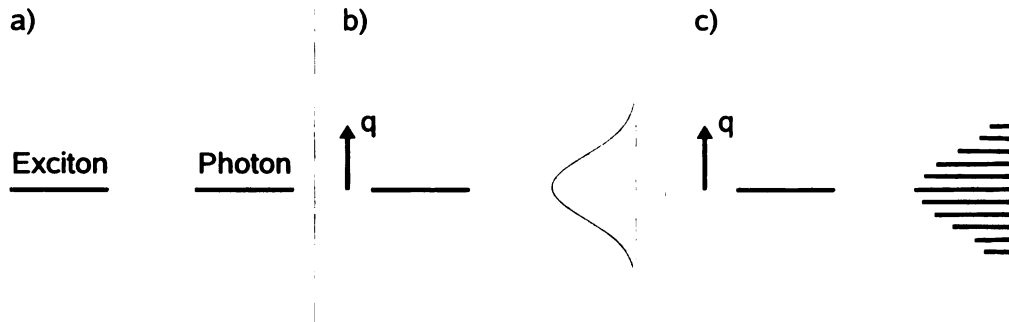


Figure 2.4. In the quantum well case there is a one to one correspondence of states in the exciton-photon interaction (a), whereas the quantum dot exciton couples to a continuous photon bath (b). The QD lattice presents an intermediate case, where the exciton couples to a infinite but discrete set of photon modes (c). In the latter two cases the coupling for large \mathbf{q} is suppressed by the form factor $\tilde{\chi}(\mathbf{q})$.

We often will refer to the picture where we consider the different photon modes as quasiparticles labelled by a quantum number \mathbf{Q} , that have an in-plane momentum \mathbf{q} , which is restricted to the first Brillouin zone. In this spirit, the umklapp photon \mathbf{Q} has an energy dispersion $\omega_{\mathbf{Q}}(\mathbf{q}) = \omega_{\mathbf{q}+\mathbf{Q}}$.

In this quasiparticle picture it is easy to prove that the quantum number \mathbf{q} is conserved. It is important to notice that this is a quasi-momentum conservation only, as the introduction of the umklapp modes is nothing but a relabeling of the modes in the reduced zone scheme of the photon dispersion (Fig. 2.5). Obviously the conservation of \mathbf{q} does not imply a in-plane momentum conservation.

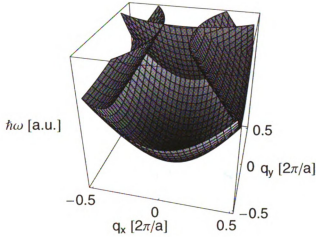


Figure 2.5. The first four photon modes in the reduced zone scheme.

2.2.1 Simplifications and Approximations

As we limit our basis to the states with one excitation only, the basis we choose consists of the ground state $|0\rangle = |0\rangle \otimes |0\rangle$ as well as the exciton state $|\mathbf{q}\rangle = |\mathbf{q}\rangle \otimes |0\rangle$ and the umklapp photon states $|1_{\mathbf{q}+\mathbf{Q},\sigma}\rangle = |0\rangle \otimes |1_{\mathbf{q}+\mathbf{Q},\sigma}\rangle$, where \mathbf{Q} runs over the reciprocal lattice and $\sigma = E, M$.

In this basis we state that the total number operator

$$\hat{N} = \hat{N}_x + \hat{N}_{em} = \sum_{\mathbf{q} \in 1.BZ} a_{\mathbf{q}}^\dagger a_{\mathbf{q}} + \sum_{\mathbf{q} \in 1.BZ} \sum_{\mathbf{Q} \in RL,\sigma} A_{\mathbf{q}+\mathbf{Q},\sigma}^\dagger A_{\mathbf{q}+\mathbf{Q},\sigma}, \quad (2.53)$$

commutes with the full Hamiltonian (2.51)

$$[H, \hat{N}] = 0. \quad (2.54)$$

Thus the eigenvalues of \hat{N} , i.e the total number of excitations, is conserved.

The first approximation affects the coupling constant for large wave vectors. Due to the finiteness of the quantum dots the coupling constant is suppressed by the form

factor $\tilde{\chi}(\mathbf{q}) = e^{-\frac{1}{4}\mathbf{q}^2\beta^2}$. Thus we introduce a cutoff wavelength Q_0 and neglect in Eq. (2.52) all parts in the sum over the reciprocal lattice vectors with $|\mathbf{Q}| > Q_0$. This approximation reduces the dimension of our system to a finite value.

Note that for point-like oscillators ($\beta \rightarrow 0$), where this cutoff is not present the contributions from all vectors \mathbf{Q} can be summed up analytically in a series [29].

Using the basis $\mathfrak{B} = \{|0\rangle, |\mathbf{q}\rangle, \{|1_{\mathbf{q}+\mathbf{Q},\sigma}\rangle, |\mathbf{Q}| < Q_0, \sigma = E, M\}\}$ the Hamiltonian $h(\mathbf{q})$ can be written in the matrix form

$$h(\mathbf{q}) = \hbar \begin{pmatrix} \omega_x & g_{\mathbf{q}}^{E*} & g_{\mathbf{q}}^{M*} & g_{\mathbf{q}+\mathbf{Q}_1}^{E*} & g_{\mathbf{q}+\mathbf{Q}_1}^{M*} & \cdots & g_{\mathbf{q}+\mathbf{Q}_n}^{M*} \\ g_{\mathbf{q}}^E & \omega_{\mathbf{q}} & 0 & 0 & 0 & \cdots & 0 \\ g_{\mathbf{q}}^M & 0 & \omega_{\mathbf{q}} & 0 & 0 & \cdots & 0 \\ g_{\mathbf{q}+\mathbf{Q}_1}^E & 0 & 0 & \omega_{\mathbf{q}+\mathbf{Q}_1} & 0 & \cdots & 0 \\ g_{\mathbf{q}+\mathbf{Q}_1}^M & 0 & 0 & 0 & \omega_{\mathbf{q}+\mathbf{Q}_1} & \cdots & 0 \\ \vdots & \vdots & \vdots & \vdots & \vdots & \ddots & \vdots \\ g_{\mathbf{q}+\mathbf{Q}_n}^M & 0 & 0 & 0 & 0 & \cdots & \omega_{\mathbf{q}+\mathbf{Q}_n} \end{pmatrix}, \quad (2.55)$$

where we have chosen an arbitrary numeration for the reciprocal lattice vectors in which \mathbf{Q}_n denotes the last vector that fulfills the condition $|\mathbf{Q}| < Q_0$.

It is possible to block diagonalize this matrix by changing the basis in the n subspaces, each spanned by the two polarisation vectors $|1_{\mathbf{q}+\mathbf{Q}_i,E}\rangle$ and $|1_{\mathbf{q}+\mathbf{Q}_i,M}\rangle$, respectively. The new basis vectors $|T_{\mathbf{q}+\mathbf{Q}_i}\rangle$ and $|L_{\mathbf{q}+\mathbf{Q}_i}\rangle$ mix the E and M polarisations and are defined as

$$|T_{\mathbf{q}}\rangle = \alpha_{\mathbf{q}} |1_{\mathbf{q},E}\rangle + \beta_{\mathbf{q}} |1_{\mathbf{q},M}\rangle \quad (2.56)$$

$$|L_{\mathbf{q}}\rangle = \beta_{\mathbf{q}} |1_{\mathbf{q},E}\rangle + \alpha_{\mathbf{q}} |1_{\mathbf{q},M}\rangle, \quad (2.57)$$

where

$$\alpha_{\mathbf{q}} = \frac{i}{\sqrt{1 + (\frac{k_z}{k})^2}} \quad (2.58)$$

$$\beta_{\mathbf{q}} = \frac{k_z/k}{\sqrt{1 + (\frac{k_z}{k})^2}}. \quad (2.59)$$

So the transformation matrix between the two basis systems has the block diagonal form

$$\mathfrak{E}_{\mathbf{q}} = \begin{pmatrix} 1 & & & & & \\ & B_{\mathbf{q}} & & & & \\ & & B_{\mathbf{q}+\mathbf{Q}_1} & & & \\ & & & B_{\mathbf{q}+\mathbf{Q}_2} & & \\ & & & & \cdots & \\ & & & & & B_{\mathbf{q}+\mathbf{Q}_n} \end{pmatrix}, \quad (2.60)$$

where the two dimensional blocks $B_{\mathbf{q}}$ are defined as

$$B_{\mathbf{q}} = \begin{pmatrix} \alpha_{\mathbf{q}} & \beta_{\mathbf{q}} \\ \beta_{\mathbf{q}} & \alpha_{\mathbf{q}} \end{pmatrix}. \quad (2.61)$$

In this new basis the Hamiltonian $\tilde{h}(\mathbf{q}) = \mathfrak{E}_{\mathbf{q}}^* h(\mathbf{q}) \mathfrak{E}_{\mathbf{q}}$ splits up into two blocks of dimension $n + 1$ and n , of which the latter is diagonal. It turns out that this diagonal block belongs to the space spanned by the n L-polarisation vectors so that these polarisations are completely decoupled from the system and thus neglected in the following.

The remaining $n + 1$ dimensional Hamiltonian has the form

$$\tilde{h}(\mathbf{q}) = \hbar \begin{pmatrix} \omega_x & g_{\mathbf{q}} & g_{\mathbf{q}+\mathbf{Q}_1} & g_{\mathbf{q}+\mathbf{Q}_2} & \cdots & g_{\mathbf{q}+\mathbf{Q}_n} \\ g_{\mathbf{q}} & \omega_{\mathbf{q}} & 0 & 0 & \cdots & 0 \\ g_{\mathbf{q}+\mathbf{Q}_1} & 0 & \omega_{\mathbf{q}+\mathbf{Q}_1} & 0 & \cdots & 0 \\ g_{\mathbf{q}+\mathbf{Q}_2} & 0 & 0 & \omega_{\mathbf{q}+\mathbf{Q}_2} & \cdots & 0 \\ \vdots & \vdots & \vdots & \vdots & \ddots & \vdots \\ g_{\mathbf{q}+\mathbf{Q}_n} & 0 & 0 & 0 & \cdots & \omega_{\mathbf{q}+\mathbf{Q}_n} \end{pmatrix}, \quad (2.62)$$

where the new coupling constant is

$$g_{\mathbf{q}} = \sqrt{1 + \left(\frac{k_z}{k}\right)^2} |g_{\mathbf{q}}^E|. \quad (2.63)$$

In the next step we show that we can safely neglect terms in the Hamiltonian that are off-resonant, i.e. for which the condition $|\omega_i - \omega_x| \gg 2g_i$ holds, where i stands for the expression $\mathbf{q} - \mathbf{Q}_i$ for a fixed \mathbf{q} .

We will calculate the energy shift due to the off-resonant modes using a perturbative approach on the quantity $x_i := \frac{2g_i}{\omega_i - \omega_x}$. Without loss of generality we assume

all off-resonant modes to have a higher energy than the exciton. The treatment of the modes below the exciton energy is analogous, with the only difference that the respective energies are shifted in the opposite direction.

In the first order in x_i the energy shift of the exciton mode can be calculated as

$$\Delta\omega_x = - \sum_i \frac{1}{2} g_i x_i + O(x_i^2), \quad (2.64)$$

and the shift in the photon energy ω_i is

$$\Delta\omega_i = + \frac{1}{2} g_i x_i + O(x_i^2), \quad (2.65)$$

Denoting with Q_0 the off-resonant photon mode with the lowest energy and thus smallest deviation from the exciton energy, we notice that $x_0 = \frac{2g_0}{\omega_0 - \omega_x}$ represents an upper boundary for the set $\{x_i\}$

$$x_i \leq x_0 \quad \forall i. \quad (2.66)$$

Since also $0 < g_i < g_{i=0} \forall i$, we can obtain an upper bound for the exciton energy shift as:

$$|\Delta\omega_x| \leq \left| \frac{m}{2} g_0 x_0 \right| + O(x_0^2), \quad (2.67)$$

where m denotes the total number of off-resonant modes which is finite due to the earlier introduced cutoff. This result holds in the case where we take into account photon modes below the exciton energy.

This approximation shows that in the system we are considering we can safely neglect the off resonant terms, as for the parameters we are using the energy deviation can be estimated to be of smaller than 0.1 meV. Note that this is a very rough estimation as we approximated the x_i by their upper bound x_0 . Numerical calculations show that the actual effect of the off-resonant modes is much smaller.

2.2.2 The Exciton at Resonance and the Strong Coupling Regime

In this section the focus lies on examining the Hamiltonian given in Eq. (2.62) at special symmetry points of the Brillouin zone. The feature that makes these points

of special interest for us is that here two or more photon modes are intersecting.

Let \mathbf{q}_0 be such a symmetry point where n photon modes intersect at energy ω . Then, by neglecting the off-resonant modes according to the previous section and assuming the system to be tuned in such a way that the exciton has an energy resonant with the intersecting photon modes, the corresponding matrix has dimension $n + 1$ and the simple form

$$\tilde{h}(\mathbf{q}_0) = \hbar \begin{pmatrix} \omega & g & g & g & \cdots & g \\ g & \omega & 0 & 0 & \cdots & 0 \\ g & 0 & \omega & 0 & \cdots & 0 \\ g & 0 & 0 & \omega & \cdots & 0 \\ \vdots & \vdots & \vdots & \vdots & \ddots & \vdots \\ g & 0 & 0 & 0 & \cdots & \omega \end{pmatrix}, \quad (2.68)$$

where $g \equiv g_{\mathbf{q}+\mathbf{Q}}$ and \mathbf{Q} is the quantum number of one of the considered photon modes.

In a procedure similar to the one used when we were dealing with the E-and M-polarisation we can reduce this matrix to the form

$$\tilde{h}(\mathbf{q}_0) = \hbar \begin{pmatrix} \omega & \sqrt{ng} & 0 & 0 & \cdots & 0 \\ \sqrt{ng} & \omega & 0 & 0 & \cdots & 0 \\ 0 & 0 & \omega & 0 & \cdots & 0 \\ 0 & 0 & 0 & \omega & \cdots & 0 \\ \vdots & \vdots & \vdots & \vdots & \ddots & \vdots \\ 0 & 0 & 0 & 0 & \cdots & \omega \end{pmatrix}. \quad (2.69)$$

We realize that in the new basis at the crossing point only one mode couples to the exciton while the remainder of the modes is left unaltered. The two dimensional matrix can easily be diagonalized and we find the eigenvalues of the whole matrix to be

$$\lambda_{1,2} = \omega \pm \sqrt{ng}, \quad (2.70)$$

as well as the $(n - 1)$ -fold degenerate eigenvalue

$$\lambda_3 = \omega. \quad (2.71)$$

That means that the Rabi splitting between the highest and the lowest mode $\Omega = 2\sqrt{n}g$ is proportional to the square root of the number of intersecting photon modes. The factor \sqrt{n} gives an important enhancement of the Rabi splitting at the lattice symmetry points. According to our assumptions at a given point \mathbf{q}_0 in the first Brillouin zone and for a given radius r we only have to consider those umklapp terms for which the Bragg-condition

$$r - \delta < |\mathbf{q}_0 + \mathbf{Q}_i| < r + \delta, \quad (2.72)$$

holds. Here δ denotes a small deviation tolerance. The number of modes that fulfill this condition for a large r in a regular lattice is proportional to r . In the limit of point-like quantum dots the form factor $\tilde{\chi}(\mathbf{q})$ reduces to 1 and the coupling constant is proportional to $\frac{1}{\sqrt{r}}$. Thus we see that for large r the factor due to the number of modes cancels the factor arising from the coupling constant.

So far we did all the calculations under the assumption that we are dealing with an ideal cavity and an exciton of infinite lifetime. We now want to include the effects of a finite lifetime of both excitons and cavity photons, due to e.g. exciton-phonon scattering processes and the imperfection of the cavity mirrors.

We therefore introduce decay factors κ for photons and γ for excitons in the Hamiltonian, which become manifest as an imaginary part of the diagonal elements [33] and subsequently solve the resulting non-hermitian eigenvalue problem.

At the crossing point of n modes the Hamiltonian then has the form

$$\tilde{h}(\mathbf{q}_0) = \begin{pmatrix} \omega + i\gamma & \sqrt{n}g \\ \sqrt{n}g & \omega + i\kappa \end{pmatrix}, \quad (2.73)$$

so that the eigenvalues can be calculated as

$$\lambda_{1,2} = \omega + \frac{1}{2}i(\gamma + \kappa) \pm \frac{1}{2}\sqrt{(2\sqrt{n}g)^2 - (\kappa - \gamma)^2}. \quad (2.74)$$

Note that additionally there is the $(n - 1)$ -fold degenerate eigenvalue $\lambda_3 = \omega + i\kappa$.

From Eq. (2.74) it follows that there is only a Rabi splitting if the condition

$$(2\sqrt{ng})^2 > (\kappa - \gamma)^2 \quad (2.75)$$

is fulfilled. In the literature, this case is called the strong coupling regime. The other case, where the root becomes purely imaginary and the real part of the eigenvalues is left unaltered is called the weak coupling regime. We assume the decay rates to be small enough to be in the strong coupling regime and neglect splitting reductions due to decay processes as they can be assumed to be small.

CHAPTER 3

Numerical Calculation

In this chapter we will present the numerical calculations we conducted in order to study the energy dispersion of the QD lattice polaritons.

In the analytical expression we provided for the coupling constant $g_{\mathbf{k}}$ in Eq. (2.63) and (2.47) there are certain constants of unknown magnitude like the relative motion wave function $\Phi_{1s}(0)$, the integral $I(\pi/L)$ and the dipole moment u_{cv} . Instead of conducting analytical estimations for these quantities we will determine them by linking our theoretical results to experimental data.

The system we consider in the following is $GaAs/Al_{0.3}Ga_{0.7}As$. This III-V compound has a refraction index of $n_r = 3.55$ in the considered wavelength range [1] and a bulk exciton resonance energy of $\hbar\omega_x = 1.515$ eV [28]. Due to the z-confinement the exciton energy in a 25 nm quantum well is increased to the value $\hbar\omega_x^{QW} = 1.525$ eV [27]. In such a QW the Rabi splitting is found to be $\Omega = 3.6$ meV [6].

In order to exploit these data we use the fact that we can recover the QW coupling constant [41] from Eq. (2.63) in the limit of one dot ($N = 1$) which covers the whole quantisation area ($\frac{\sqrt{2\pi\beta}}{\sqrt{S}} \rightarrow 1$). Moreover, it is necessary to replace the QW by the QD exciton energy, which has been found for lens shaped dots of radius $R_0 = 50$ nm to be $\hbar\omega_x^{QD} = 1.68$ eV [18].

Therefore, using the fact that the coupling is proportional to the exciton energy,

we find the relation

$$g_{\mathbf{k}} = \frac{\omega_x^{QD}}{\omega_x^{QW}} \sqrt{n} \sqrt{2\pi} \beta e^{\frac{1}{4}\beta^2 q^2} g_{\mathbf{k}}^{QW}, \quad (3.1)$$

where $g_{\mathbf{k}}^{QW}$ can be written as

$$g_{\mathbf{k}}^{QW} = \sqrt{1 + \left(\frac{k_z}{k}\right)^2} \frac{\nu}{\sqrt{k} \sqrt{L_{eff}}}. \quad (3.2)$$

Here, ν stands for all the remaining constants, including the unknown quantities $\Phi_{1s}(0)$, $I(\pi/L)$ and u_{cv} .

Note that the cavity length L has to be replaced by an effective width $L_{eff} = 2L + L_{DBR}$ which arises from the imperfection of the cavity mirrors and the resulting finite penetration depth of the electric field in the mirrors [39]. L denotes the resonance length of an ideal $\lambda/2$ cavity. L_{DBR} can be calculated by an exact transfermatrix calculation for the modes of a real cavity. We use the value L_{DBR} from [39] which is sufficiently accurate for our purpose.

By comparison with the experimental data we find a value for the effective constant ν of $h\nu = 8.09$ meV.

In the following sections we are going to examine the dispersion modes for a square and a hexagonal lattice, which are obtained by a numerical diagonalization using generalized Hopfield transformations. These transformations are implicitly applied in the diagonalization of the matrix in Eq. (2.62). After having calculated the eigenvalues numerically the Hamiltonian can be written in the form

$$H = \sum_{\mathbf{q}, \xi} \hbar \omega_p^{\xi}(\mathbf{q}) p_{\mathbf{q}, \xi}^{\dagger} p_{\mathbf{q}, \xi}, \quad (3.3)$$

where $\hbar \omega_p^{\xi}(\mathbf{q})$ denotes the ξ^{st} eigenvalue and $p_{\mathbf{q}, \xi}^{(\dagger)}$ is the polariton creation (annihilation) operator.

We have to stress that the latter form of the Hamiltonian was derived under the assumption of a system with a single excitation. In order to expand this result to the

many body problem of a highly excited system, a careful investigation of the polariton commutator relations is necessary.

Since the polariton operator is composed by the exciton and photon operators as

$$p^\dagger = \alpha_x a^\dagger + \sum_{\mathbf{Q}} \alpha_{ph\mathbf{Q}} A_{\mathbf{Q}}^\dagger, \quad (3.4)$$

the commutator can be calculated as

$$[p, p^\dagger] = |\alpha_x|^2 [a, a^\dagger] + \sum_{\mathbf{Q}} |\alpha_{ph\mathbf{Q}}|^2. \quad (3.5)$$

Therefore, in the case of very large dots, in which the bosonic approximation holds and $[a, a^\dagger] \approx 1$ the polaritons approximately behave as bosons too and their operators fulfill

$$[p_{\mathbf{q},\xi}, H] = \hbar\omega_p^\xi(\mathbf{q}) p_{\mathbf{q},\xi}. \quad (3.6)$$

Thus, the Hamiltonian is diagonal in terms of the polariton operators $p_{\mathbf{q},\xi}$ and $p_{\mathbf{q},\xi}^\dagger$ and the eigenstates of the system can be written as a Fock state

$$|n_{\alpha_1}, n_{\alpha_2}, \dots\rangle = \frac{1}{\sqrt{n_{\alpha_1}! n_{\alpha_2}! \dots}} \left(p_{\alpha_1}^\dagger\right)^{n_{\alpha_1}} \left(p_{\alpha_2}^\dagger\right)^{n_{\alpha_2}} \dots |\phi_0\rangle, \quad (3.7)$$

where α_i denotes an arbitrary pair (\mathbf{q}, ξ) .

This is not true if the exciton operators show a remarkable deviation from bosonic behaviour.

3.1 Preliminary Discussion

In this section we will exemplarily present the conducted preparatory calculations for the case of a quantum dot square lattice, before we turn to the actual numerical calculation of the polariton modes. An analogous calculation has been carried out for the hexagonal lattice.

The simple square Bravais lattice, with square primitive cell of side a , has as its reciprocal another simple square lattice, but with square primitive cell of side $2\pi/a$.

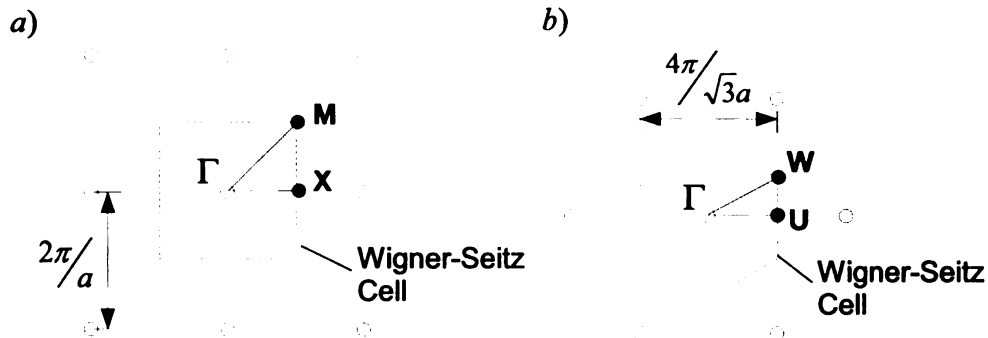


Figure 3.1. The reciprocal lattice:(a) of a square lattice with lattice constant a and (b) of a hexagonal lattice with constant a . As usual Γ denotes the origin $\mathbf{q} = 0$.

In the reciprocal space there are two symmetry points that are of special interest, the X-point, which has a π -rotational symmetry and the M-point, which has a $\pi/2$ -rotational symmetry (Fig. 3.1 a)).

After having linked the constants in our theory to the experimental data in the previous section, we can finally write down the coupling constant for the $GaAs/Al_{0.3}Ga_{0.7}As$ system as

$$g_{\mathbf{q}} = \nu \sqrt{n} \frac{\sqrt{2\pi}\beta}{\sqrt{2L + L_{DBR}}} \frac{1}{\sqrt{k}} \sqrt{1 + \left(\frac{k_z}{k}\right)^2} e^{-\frac{1}{4}\beta^2 q^2}, \quad (3.8)$$

where $\hbar\nu = 8.09$ meV.

At first, we try to optimize the system parameters with regard to the coupling strength at resonance. The free parameters in our system are the quantum dot radius $R_0 = \beta/\sqrt{2}$, the length of the ideal cavity L and finally the lattice constant a , which determines the dot density n as well as the size of the Brillouin zone.

Generally, at a point in the reciprocal lattice \mathbf{q}_0 where two or more photon modes \mathbf{Q}_i intersect the Bragg-condition

$$|\mathbf{Q}_i + \mathbf{q}_0| = d \quad \forall i, \quad (3.9)$$

is satisfied for a constant d (Fig. 3.9). Our purpose is to maximize the coupling constant at this distance d in order to achieve the largest possible Rabi splitting.

Exploiting the fact that the photon energy has to match the exciton energy at the crossing point

$$\hbar\omega_x = 1.68 \text{ meV} = \hbar \frac{c}{n_r} \sqrt{d^2 + \left(\frac{\pi}{L}\right)^2}, \quad (3.10)$$

and by expressing d in units of the reciprocal lattice constant $d = \tilde{d} \frac{2\pi}{a}$ we find a functional dependence of the coupling constant for a fixed exciton energy $\hbar\omega_x = 1.68 \text{ meV}$ which is independent of the lattice constant a

$$g_d = \frac{1}{\tilde{d}} f(\beta, L), \quad (3.11)$$

where we excluded the special case $\tilde{q} = 0$.

Thus we only have to optimize the function f with regard to the remaining free parameters of the system, which are the dot radius $R_0 = \sqrt{2}\beta$ and the cavity length L . A two dimensional plot of $f(\beta, L)$ is given in Fig. 3.2.

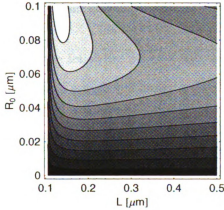


Figure 3.2. The function $f(\beta, L)$. The light regions correspond to higher values.

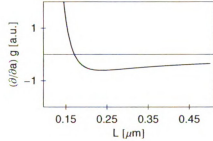


Figure 3.3. Plot of the derivative of $f(R_0/\sqrt{2}, L)$ with respect to L for a fixed $R_0 = 50 \text{ nm}$. Notice that the coupling is maximal for a value of $L = 0.171 \mu\text{m}$.

For a fixed radius of $R_0 = 50 \text{ nm}$ we find the optimal value for the cavity length to be $L = 0.171 \mu\text{m}$ (Fig. 3.3). According to Eq. (3.11) this value for L is optimal independently of the crossing point under consideration. We find a simple expression

for the coupling constant at the resonance point that only depends on \tilde{d}

$$g_d = \frac{1}{\tilde{d}} g_0, \quad (3.12)$$

where $g_0 = 0.387$ meV for the optimized values. From this equation we can calculate according to Eq. 2.70 the expected half Rabi splitting $\Omega/2$ for different symmetry points of the 1st BZ by multiplying g_d with the square root of the number of intersecting photon modes. In Tab. 3.1 the calculated values for the Rabi splitting at the symmetry points of the square lattice are listed.

	X	K1	K2
\tilde{d}	1/2	$\sqrt{2}$	$\sqrt{5/2}$
#modes	2	4	8
Ω	2.19meV	2.19meV	1.385 meV

Table 3.1. The Rabi splitting Ω depends on the relative size of the wave vector \tilde{d} at the crossing point and the number of intersecting modes.

In the following we are going to turn our attention to the polariton modes in the vicinity of a high symmetry point.

3.2 Square Lattice: The X-Point

At first, we will focus on the X-point at $\mathbf{q}_0 = (\pi/a, 0)$ of the reciprocal space of a square lattice with constant a (Fig. 3.1). For the calculation we included all umklapp terms in the Hamiltonian of Eq. (2.62) up to a certain cutoff length due to the form factor $\tilde{\chi}(\mathbf{q})$. Furthermore, we dropped the completely decoupled L-photon modes.

At the X-point, the lowest photon modes crossing are arising from the original photon mode ($\mathbf{Q} = 0$) and the umklapp term with $\mathbf{Q} = (-2\pi/a, 0)$. Speaking in the quasiparticle picture, these two photon modes have the same energy at the edge of the Brillouin zone at $\mathbf{q}_0 = (\pi/a, 0)$. We will present the calculations of the polariton

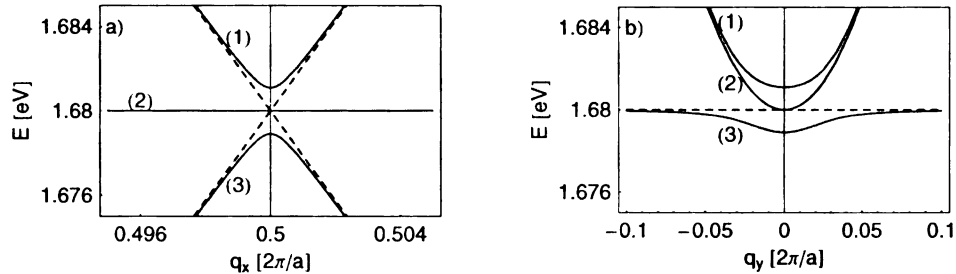


Figure 3.4. The polariton modes (1)-(3) at the X-point along $\overline{\Gamma X}$ (a) and along \overline{XM} (b). The upper polariton (1) has a local minimum and can thus be considered as a quasiparticle with a positive effective mass. The dashed lines represent the unperturbed modes.

dispersions and properties using the optimal parameters calculated in the previous section.

For the lowest crossing at the X-point, where $\bar{d} = 1/2$, the corresponding lattice constant we have to choose according to Eq. (3.10) is $a = 0.131 \mu\text{m}$. Using these parameters we find the polariton dispersions in the vicinity of \mathbf{q}_0 in Fig. 3.4, which shows the modes along the q_x - and q_y -axis, respectively.

As predicted, we find at the crossing point a Rabi splitting of about 2.2 meV between the upper (UP) and the lower (LP) polariton mode.

The energy of the lower polariton mode has a saddle point at \mathbf{q}_0 and thus the assignment of an effective mass is not well defined. The upper (1) as well as the central (2) polariton, however, show a local minimum at the X-point. The upper polariton mode is shown in a two dimensional plot in Fig. 3.5.

The π -rotational symmetry of the X-point is reflected in the energy dispersion, which has a very different appearance along the q_x - and q_y -directions. This property can be checked numerically by calculating the effective masses of the polariton modes. The effective mass of a quasiparticle is defined only at a local minimum or maximum of the mode as

$$(m_i^*)^{-1} = \frac{1}{\hbar^2} \frac{\partial^2 E_i(\mathbf{q})}{\partial \mathbf{q}^2}. \quad (3.13)$$

It describes the behaviour of the mode in the direct vicinity of the extremum. The cal-

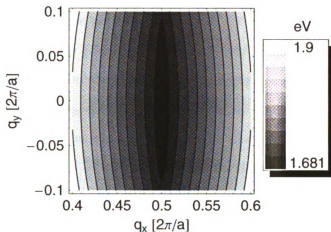


Figure 3.5. The upper polariton dispersion at the X-point. Because of the special π -rotational symmetry of this point the dispersion has a valley at the edge of the Brillouin zone.

culated effective masses for the polariton modes (1) and (2) can be found in Tab. 3.2. The masses are expressed in units of the of the cavity photon in-plane effective mass

	UP (1)	CP (2)
m_{xx}/m_{ph}	$1.7 \cdot 10^{-3}$	0.44
m_{yy}/m_{ph}	3.32	1.24

Table 3.2. The effective masses for the upper two polariton modes at X. The masses are expressed in units of the photon effective mass in a ideal cavity of length $L = 0.171 \mu\text{m}$ ($m_{ph} = 2.52 \cdot 10^{-5} m_0$).

in the lowest mode ($k_z = \frac{\pi}{L}$) at $\mathbf{q} = 0$ in an ideal cavity of length L . This mass can be calculated as $m_{ph} = \hbar \frac{n_r \pi}{cL} = 2.52 \cdot 10^{-5} m_0$, where m_0 denotes the electron rest mass.

As suggested by Fig. 3.5 the upper polariton mass is extremely small in the q_x -direction (about $10^{-3} m_{ph}$), while in the q_y -direction it is of the order of the photon effective mass. The latter also is of the same order of magnitude as the effective mass of quantum well polaritons [15].

An explanation of this behaviour is given in the expansion of the unperturbed cavity photon modes at the point $\mathbf{q}_0 = (\pi/a, 0)$. The leading term in the cavity modes along the q_y -axis is (disregarding the constant term) is of quadratic order, while along the q_x -direction the linear term dominates. This accounts for the fact that the effective mass in q_x -direction is approximately by a factor $\sqrt{2\bar{g}}$ smaller than the mass in q_y -direction, as an expansion of the polariton energies in q_x and q_y shows. \bar{g} is defined as $\bar{g} = \frac{gq_0}{\omega_x}$ and has for typical constants for the system under consideration a value of the order of 10^{-3} .

The anisotropy of the polariton modes is a direct consequence of the π -rotational symmetry of the X-point. So, in order to find polariton states with an isotropic mass, which is important with regard to condensation effects we will discuss later, we have to consider a point with higher symmetry like the M-point of the square lattice or the W-point of the hexagonal lattice, which have an $\pi/2$ - and $2\pi/3$ -rotational symmetry, respectively. Before we are discussing these highly symmetric points we will closer

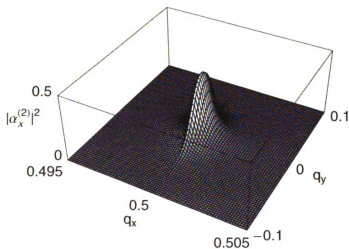


Figure 3.6. The exciton component of polariton mode (1) $|\alpha_x^{(1)}(\mathbf{q})|^2$. Only in the direct vicinity of \mathbf{q}_0 the upper polariton becomes excitonic.

examine the polariton modes at the X-point.

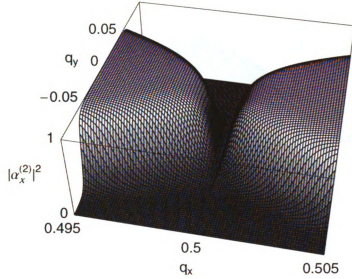


Figure 3.7. The exciton component of mode (2) $|\alpha_x^{(2)}(\mathbf{q})|^2$. Remarkably this mode is purely photonic on the edge of the Brillouin zone.

Since in the vicinity of \mathbf{q}_0 the polariton states can be expressed as a linear combination of the exciton state and the two photon states,

$$\left|P_{\mathbf{q}}^{\xi}\right\rangle = \alpha_x^{\xi}(\mathbf{q})|\mathbf{q}\rangle + \alpha_{ph1}^{\xi}(\mathbf{q})\left|T_{\mathbf{q}}^{\mathbf{Q}=0}\right\rangle + \alpha_{ph2}^{\xi}(\mathbf{q})\left|T_{\mathbf{q}}^{\mathbf{Q}=(-1,0)}\right\rangle, \quad (3.14)$$

we can keep track of the excitonic and photonic parts in the new eigenmodes.

In Figs. 3.6-3.8 the excitonic part $|\alpha_x^{\xi}(\mathbf{q})|^2$ of the three polariton modes ($\xi = 1, 2, 3$) is depicted. Since the polariton state is normalized to one, the photonic part $|\alpha_{ph1}^{\xi}(\mathbf{q})|^2 + |\alpha_{ph2}^{\xi}(\mathbf{q})|^2$ appears as the negative of the Figs. 3.6-3.8.

We see that near resonance we have a strong mode mixing between photons and excitons. At resonance, the upper and the lower polariton are exactly half excitonic and half photonic, whereas the center mode is purely photonic. This is a remarkable result, because although the center mode has exactly the exciton energy at resonance the corresponding eigenstate is purely photonic.

Note that the center mode's deviation from the unperturbed exciton mode in Fig. 3.4 along the q_x direction is too small to be seen on this scale. But in fact

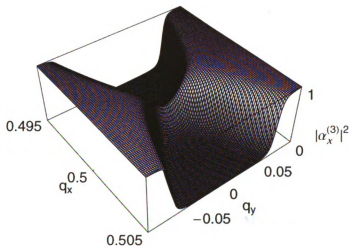


Figure 3.8. The exciton component of mode (3) $|\alpha_x^{(3)}(\mathbf{q})|^2$. At resonance this mode is half excitonic half photonic.

the mode has a local minimum at \mathbf{q}_0 with photon-like effective masses in q_x - and q_y -direction, respectively (Tab.3.2).

Moreover the x-y asymmetry of X is once again reflected in Fig. 3.7. While in q_x -direction the central mode returns to its excitonic nature very quickly, it remains purely photonic in the q_y -direction on the edge of the Brillouin zone.

Note that except for the well localized region around \mathbf{q}_0 , Fig. 3.7 is the negative of Fig. 3.8. At the edges where the two modes change their nature from excitonic to photonic and vice versa the unperturbed exciton mode intersects a single photon mode. At this intersection points, the polariton modes behave similar to bulk polaritons depicted in Fig. 1.3.

We summarize that we have created a novel kind polariton states at the edge of the Brillouin zone, i.e. they have, unlike quantum well polaritons, a finite momentum. This is associated with interesting effects in the interaction with external photon modes. These effects will be discussed later in section 3.5. Moreover, we found that

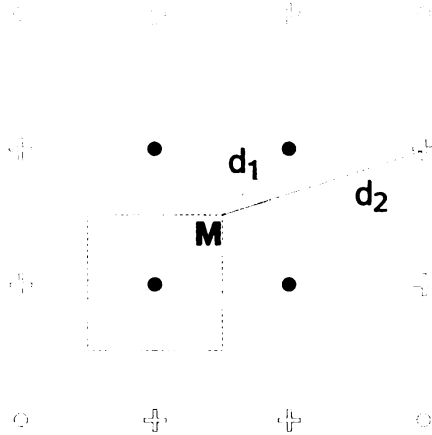


Figure 3.9. At the M point we distinguish two cases. M1 labels the crossing, where the closest photon modes intersect (black dots). At the M2 crossing the second closest photon modes intersect (crosses). The different modes fulfill $|\mathbf{Q}_i + \mathbf{q}_0| = d_{1/2}$ for the two cases, respectively.

the upper polaritons have a photon like effective mass along the zone boundary, as usual QW polaritons, but along the q_x -direction we find an exceptionally small mass, which is by a factor of 10^{-3} smaller than the QW polariton mass.

3.3 Square Lattice: The M-Point

At the M-point we are going to examine not only the lowest crossing (M1) but also the second lowest crossing (M2) (Fig. 3.9).

The M-point has a $\pi/2$ -rotational symmetry with regard to the reciprocal lattice. We therefore expect the effective mass tensor to be isotropic. Moreover the higher symmetry leads to the fact that at the lowest crossing point (M1) four photon modes ($\mathbf{Q}_1 = 0$, $\mathbf{Q}_2 = (-2\pi/a, 0)$, $\mathbf{Q}_3 = (-2\pi/a, -2\pi/a)$, $\mathbf{Q}_4 = (0, -2\pi/a)$) are intersecting instead of two at the X-point. In order to tune the intersection to the exciton energy we have to choose a lattice spacing of $a = 0.185 \mu\text{m}$ if we keep the remaining parameters in their optimal ratio ($R_0 = 0.05 \mu\text{m}$ and $L = 0.171 \mu\text{m}$).

Fig. 3.10 displays the polariton modes along the path $\overline{\Gamma M}$. Note that the central

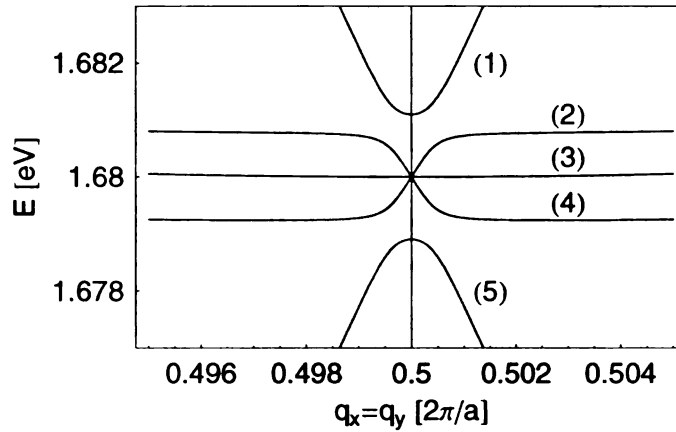


Figure 3.10. The polariton modes at the lowest crossing point at M (M1). The modes are displayed along the path $\overline{\Gamma M}$

mode (3) is an unperturbed photon mode, as along this path the energy of photon Q_2 and Q_4 is identical and thus we can introduce a basis in the respective subspace with one completely decoupled state (Section 2.2.1).

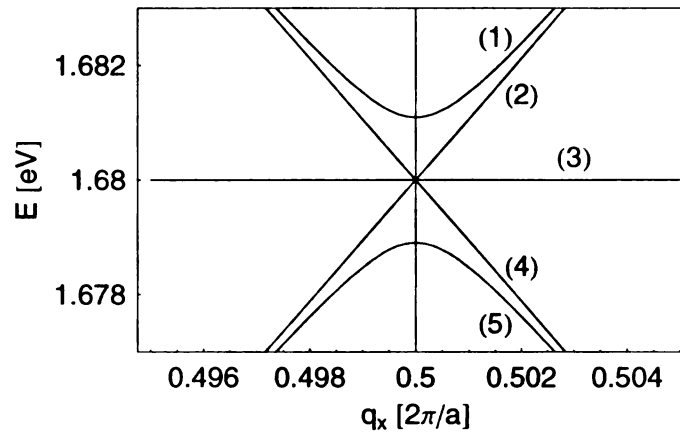


Figure 3.11. The polariton modes at the lowest crossing point at M. The modes are displayed along a path parallel to the q_x -axis. Due to the symmetry we find the same energy dispersions along the q_y -axis

Along a path parallel to the q_x -axis we find two unperturbed photon modes ((2) and (4)) which arise because of the degeneracy of energy of the photons Q_2 and Q_3 as well as Q_1 and Q_4 (Fig. 3.11).

Note that the increased number of intersecting modes compensates exactly the effect of a decreased coupling constant, when we go from the X to the M point. Thus, we find a Rabi splitting of $\Omega = 2.19$ meV like in the case of the X-point. Our main interest lies on the first polariton mode because it has a positive isotropic effective mass. This mode is depicted in Fig. 3.12 in the vicinity of \mathbf{q}_0 .

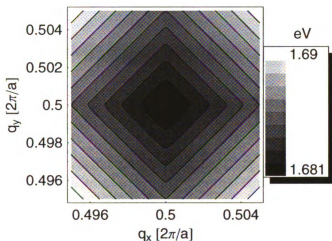


Figure 3.12. The upper polariton mode at M1. The energy dispersion is symmetric in q_x - and q_y -direction.

The mode is half excitonic and half photonic at resonance (\mathbf{q}_0) and becomes purely photonic away from \mathbf{q}_0 , as can be seen in Fig. 3.13.

The LP mode (5) has a strong resemblance with the UP mode (1). The energy dispersions show the same shape and symmetry, with the difference that at \mathbf{q}_0 we find a local maximum for the LP mode, while there is a local minimum for the UP mode. The excitonic part of the LP in the vicinity of the resonance point is almost identical to the one of the UP 3.13.

As we expected the polaritons show a dispersion that is symmetric in rotations about $\pi/2$ like the lattice itself and we find an isotropic mass tensor as the calculation of the effective masses at the M1 point shows (Tab. 3.3). Note that all the polariton

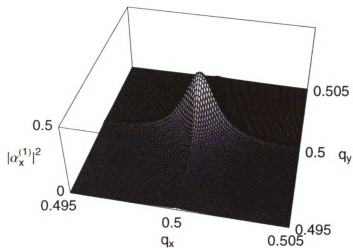


Figure 3.13. The exciton component of mode (1) at M1 $|\alpha_x^{(1)}(\mathbf{q})|^2$. At resonance this mode is half excitonic half photonic. An almost identical figure is found in the case of the lower polariton (5).

masses at M are of the order of $10^{-3} m_{ph}$, which is 10^{-3} times smaller than the usual QW polariton mass.

Next we will turn to the M2 crossing where eight photon modes intersect as depicted in Fig. 3.9. We calculated that in this case the increase of modes is not able to compensate the reduced coupling constant completely (Tab. 3.1). Instead we expect a Rabi splitting reduced by the factor $\sqrt{\frac{2}{5}}$ of $\Omega = 1.385$ meV. This is depicted in Fig. 3.14.

Again we focus on the upper polariton mode for which we find a very isotropic dispersion relation (Fig. 3.15) with an positive effective mass of $m = 2.08 \cdot 10^{-3} m_{ph}$, which is even smaller than the mass at M1 (Tab. 3.3). By keeping track of the excitonic part of the mode in Fig. 3.16 we find that the magnitude of exciton component is equal to the one of the photon component at resonance but then drops quickly to zero at higher distances.

	M1		M2	
	UP (1)	LP (5)	UP (1)	LP (9)
m_{xx}/m_{ph}	$3.43 \cdot 10^{-3}$	$-3.4 \cdot 10^{-3}$	$2.08 \cdot 10^{-3}$	$-2.06 \cdot 10^{-3}$
m_{yy}/m_{ph}	$3.43 \cdot 10^{-3}$	$-3.4 \cdot 10^{-3}$	$2.08 \cdot 10^{-3}$	$-2.06 \cdot 10^{-3}$

Table 3.3. The effective masses for the upper (UP) and the lower polariton (LP) at M1 and M2. The masses are expressed in units of the photon effective mass in a ideal cavity of length $L = 0.171 \mu\text{m}$ ($m_{ph} = 2.52 \cdot 10^{-5} m_0$).

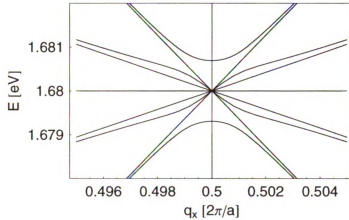


Figure 3.14. At M2 eight photon modes are crossing. The resulting nine polariton modes are displayed along the q_x -direction. Note that along this path the unperturbed photon modes can be grouped in degenerate pairs.

Like in the case of the M1 point the LP mode bears a strong resemblance to the UP mode, which is indicated by the almost identical magnitude of the effective masses in both cases 3.3. Also, the lower mode shows the same shape and symmetry as the UP in both the energy dispersion and the excitonic component. (Figs. 3.15 & 3.16).

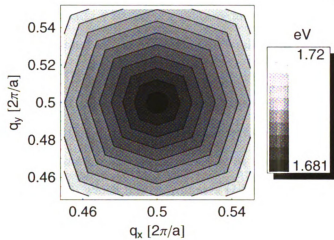


Figure 3.15. The highest polariton mode at M2. The large number of interacting photon modes provides a high symmetry of the dispersion.

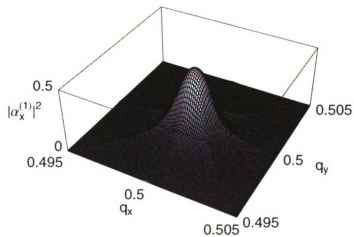


Figure 3.16. The exciton component of the highest mode at M2 $|\alpha_x(\mathbf{q})|^2$. At resonance this mode is half excitonic half photonic. We find an almost identical figure in the case of the LP.

3.4 Hexagonal Lattice: The W-Point

In this section we will consider a lattice of quantum dots in a hexagonal arrangement. A two dimensional hexagonal lattice is made up of equilateral triangles and can thus be characterized by the two primitive vectors $\mathbf{a}_1 = (a, 0)$ and $\mathbf{a}_2 = (a/2, \sqrt{3}a/2)$, where the lattice constant a denotes the distance between two neighboring lattice points. The reciprocal lattice is again a hexagonal lattice with lattice constant $a^* = \frac{4\pi}{\sqrt{3}a}$. We are going to examine the lowest crossing at the so called W point of the reciprocal lattice (Fig. 3.1), which has coordinates $(1/2, 1/(2\sqrt{3}))$, in units of a^* . At this point there are three photon modes crossing.

Also for the hexagonal lattice the coupling has a maximum for a dot radius of 50 nm, if the cavity length has the value $L = 0.171 \mu\text{m}$. This corresponds to a lattice constant of $a = 0.175 \mu\text{m}$ and thus a optimal dot density of $n = 37.8 \frac{1}{\mu\text{m}^2}$. For these optimized values we find a Rabi splitting of $\Omega = 2.16 \text{ meV}$. The polariton modes along

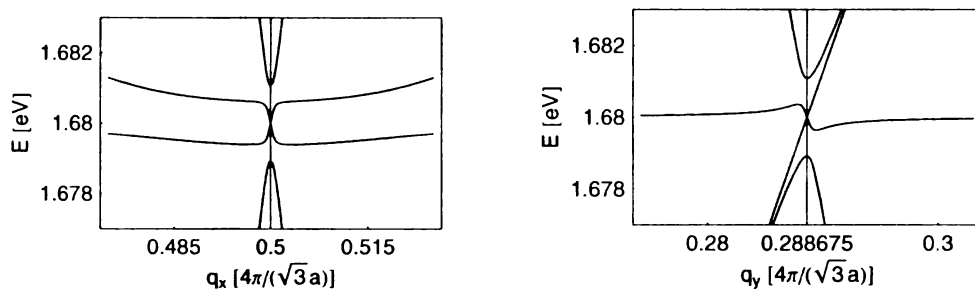


Figure 3.17. The polariton modes at the W-point of the hexagonal lattice along the x-direction (a) and the y-direction (b) are displayed.

the q_x - and q_y -axis, respectively, are depicted in Fig. 3.17. Note that the dispersion relations along the q_x -axis are even functions, while in q_y -direction they are odd.

The highest polariton mode has an local minimum at the resonance point (Fig. 3.18) and we find isotropic effective masses of $2.52 \cdot 10^{-3} m_{ph}$ and $-2.51 \cdot 10^{-3} m_{ph}$ for the highest and lowest mode, respectively. The excitonic character of the mode has a strong resemblance to the modes in the previous cases (Fig. 3.19).

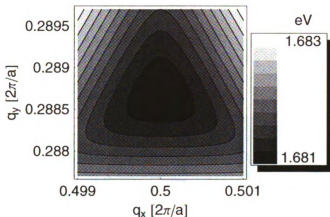


Figure 3.18. The highest polariton mode at the W-point of the hexagonal lattice.

One can clearly see that the excitonic component survives over a long range in the directions where there is no nearest neighbor reciprocal lattice vector present. As expected the $2\pi/3$ -rotational symmetry is reflected both in Figs. 3.18 and 3.19.

In the case of the W-point of the hexagonal lattice another interesting effect appears. While at the symmetry points of the square lattice the lower mode bore a strong resemblance (in shape and symmetry) with the upper mode, in the case of the hexagonal lattice the lower mode, still having a similar shape, is rotated by an angle π (Fig. 3.20). The same effect can be seen for the excitonic part of the LP in Fig. 3.21.

This mismatch in the upper and lower dispersion as well as the excitonic components is likely to suppress the polariton scattering between these two modes as polaritons can only scatter to states with a significant exciton component. In order to confirm this assumption detailed investigations on the polariton dynamics of the system are necessary.

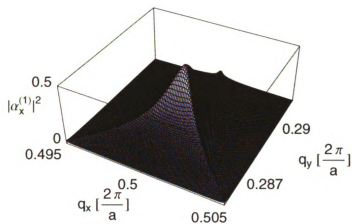


Figure 3.19. The exciton component of the highest mode at W in the hexagonal lattice $|\alpha_x(\mathbf{q})|^2$. At resonance this mode is half excitonic half photonic.

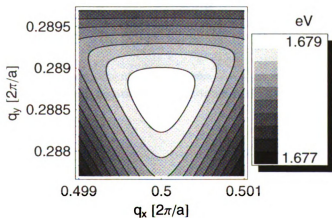


Figure 3.20. The lowest polariton mode at the W-point of the hexagonal lattice. Note that it is rotated by π with regard to the upper polariton mode.

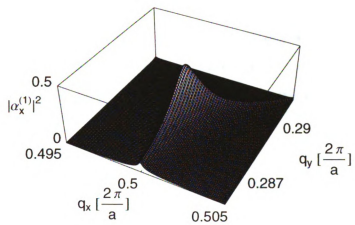


Figure 3.21. The exciton component of the lowest mode at W in the hexagonal lattice $|\alpha_x(\mathbf{q})|^2$. It is rotated by π with regard to the excitonic part of the upper mode.

3.5 Dark Polariton States

Unlike quantum well polaritons, which can have a momentum in the direct vicinity of zero only, the novel microcavity polaritons described in the previous sections have a large in-plane momentum, being located at the edge of the Brillouin zone of the reciprocal lattice. This leads to interesting effects that become manifest in the interaction with external photons in a material of refraction index n_{ext} , smaller than the refraction index of the cavity spacer n_r . Due to a total internal reflection of the polaritons at the edge of the Brillouin zone their spontaneous emission lifetime is expected to be greatly enhanced.

In the following we keep the basis determined by the microcavity symmetry, where \mathbf{q} and k_z are the components of the wave vector parallel and perpendicular to the mirrors, respectively. Since the external photons have an energy dispersion

$$E = \hbar \frac{c}{n_{ext}} \sqrt{q^2 + k_z^2}, \quad (3.15)$$

it is clear that the function $E(k_z = 0) = \hbar \frac{c}{n_{ext}} q$ represents a lower boundary for the energies accessible to the external photons (Fig. 3.22).

Let us consider polaritons at a symmetry point \mathbf{q}_0 on the edge of the Brillouin zone. These polariton states are partially in the non accessible region of the external photons, if the polariton energy at the edge $E_P(\mathbf{q}_0)$ is smaller than the lowest external photon energy $E_{ext}(\mathbf{q}_0, k_z = 0) = \hbar \frac{c}{n_{ext}} q_0$.

By approximating the polariton energy with the unperturbed cavity photon energy $E_P(\mathbf{q}_0) \approx E_{int}(\mathbf{q}_0) = \hbar \frac{c}{n_r} \sqrt{q_0^2 + (\frac{\pi}{L})^2}$, this condition reads

$$\hbar \frac{c}{n_{ext}} q_0 > \hbar \frac{c}{n_r} \sqrt{q_0^2 + (\frac{\pi}{L})^2}, \quad (3.16)$$

which can be rewritten as a condition on the refraction indices as

$$n_{ext} < \alpha n_r, \quad (3.17)$$

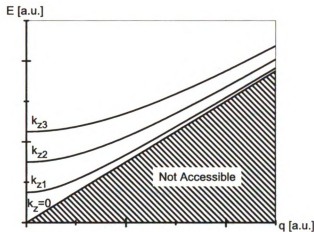


Figure 3.22. The dispersion for external photons for several arbitrary values of the (continuous) parameter k_z . The dispersion for $k_z = 0$ imposes a lower boundary for the energies accessible to free photons.

where $\alpha = 1/\sqrt{1 + (\frac{\pi}{Lq_0})^2}$.

If this condition is fulfilled there are polariton modes in the vicinity of \mathbf{q}_0 that do not couple to the external photons due to selection rules imposed by the conservation of energy and in-plane momentum (Fig. 3.24). This effect can be seen as a total internal reflection for microcavity polaritons for a large in-plane momentum \mathbf{q} .

The primary decay process of polaritons is the coupling to the external photon bath, which gives rise to a short polariton lifetime in quantum wells of the order of a few picoseconds. If polaritons are unable to decay to external photons due to their total internal reflection, we expect their spontaneous emission lifetime to be greatly enhanced.

Although the spontaneous emission lifetime of these QD lattice polaritons can be greatly enhanced using this total internal reflection, we have to note critically that there are other decay processes that come into play, such as polariton-phonon or polariton-polariton scattering.

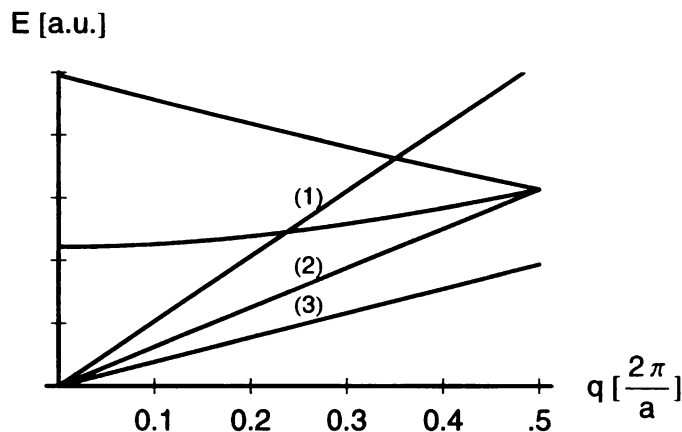


Figure 3.23. The boundary between states accessible for external photons in the reduced zone scheme for the unperturbed cavity modes in the cases (1) $n_{ext} < \alpha n_r$, (2) $n_{ext} = \alpha n_r$ and (3) $n_{ext} > \alpha n_r$. Moreover, the figure shows the lowest 2 cavity photon modes along \overline{OX} of the square lattice.

In fact, the upper polariton modes we are discussing do not represent the lowest state of the system. While the scattering processes into the central modes are likely to be strongly suppressed due to the purely photonic nature of these modes at resonance, the scattering to the lower polariton mode may significantly reduce the polariton lifetime.

This effect is not present if we consider polaritons in the lowest mode. These polaritons have a negative isotropic mass of the same magnitude of the upper polaritons. The lower polaritons do not relax to lower and lower energies, but they tend to accumulate at a certain value of q . This is due to the so called bottleneck effect, which is a consequence of the vanishing excitonic part in the polariton state away from the resonance point [48]. The polaritons lose their ability to scatter when their excitonic nature decreases. At these accumulation points (e.g. along the excitonic branches in Fig: 3.21) we expect a very long polariton lifetime and a population buildup.

In order to study these accumulation effects or to determine the actual lifetime of QD lattice polaritons a careful study of the polariton dynamics is necessary and we expect this to be subject of future investigations.

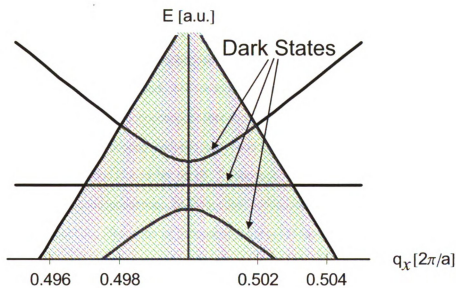


Figure 3.24. If the condition $n_{ext} < \alpha n_r$ is fulfilled there are polariton modes in the dark region (shaded area). These states do not couple to external photons and are thus expected to have a greatly enhanced lifetime.

Conclusion

In recent years, the field of quantum phase transitions in solids (such as Bose-Einstein condensation (BEC), Berezinskii-Kosterlitz-Thouless transition (KBT), or superfluidity) has attracted remarkable attention as it brings quantum mechanical effects to a macroscopic scale. In particular, microcavity polaritons are promising candidates for the observation of a phase transition into a coherent light-matter condensed phase, because in certain limits they behave as a non-interacting Bose gas. Moreover, their extremely light mass of the order of 10^{-5} electron masses, suggests the possibility of high temperature condensation. In fact, the critical temperature T_c of a BEC in an ideal, non-interacting Bose gas is inversely proportional to the particle mass [42]

$$k_B T_c = \frac{2\pi\hbar^2}{m} \left(\frac{n}{2.612} \right)^{2/3}. \quad (3.18)$$

As discussed by Imamoglu et al. in Ref. [22], microcavity polaritons might undergo BEC. This has stimulated extensive experimental studies [3, 14, 24, 32] and controversial theoretical discussions [42, 45]. Undoubtedly, some recent experiments show evidence of some type of condensation of polaritons in semiconductor heterostructures, but up to now it is unclear what the nature of the observed coherence phenomena is.

Most theoretical works agree that the ideal BEC theory is not applicable for several reasons. Aside from the fact that the claim of the bosonic nature for polaritons holds only in the low excitation limit (which is highly questionable in the context of condensation effects), the most striking argument is that in a two dimensional system, like the ones studied in the cited experiments, the critical density above

which BEC occurs diverges for every finite temperature. For interacting particles this is a direct consequence of the Mermin-Wagner theorem [30]. Thus, theoretically BEC in a two dimensional system occurs at zero temperature only. Moreover, BEC theory describes always a system in thermal equilibrium, which is in direct contradiction with the short lifetime of polaritons (of the order of a few picoseconds). Snoke therefore proposed [45] to consider the observed effects rather within the more general concept of a spontaneous emergence of coherence. Nevertheless, disregarding this questions of terminology, the mentioned experimental data clearly proves the existence of some kind of condensation effect for microcavity QW polaritons in quantum well structures.

In this thesis we presented a study of polariton modes of a novel kind, for which we propose the name of *umklapp polaritons*, as they arise from and umklapp scattering of excitons and photons. The investigated umklapp polaritons are the eigenstates of a periodic array of lens shaped GaAs quantum dots within a microcavity in the strong coupling regime. This system is of special interest as it represents an intermediate case between the limits of a zero dimensional quantum dot on the one hand, and of a two dimensional quantum well on the other. The translational symmetry of the QW case, which is lost in the case of one QD, is partially recovered in a QD lattice.

Before turning to the actual physical system we reviewed in Chapter 1 the fundamental concepts needed throughout this thesis.

In Chapter 2, we provided a full quantum mechanical treatment of the system under consideration. It turned out that, due to the periodicity of the system, the exciton states have a quantized center-of-mass motion with an in-plane momentum which is restricted to the first Brillouin zone of the reciprocal QD lattice. We have seen that these new exciton states behave like quasiparticles of infinite mass. The quantized center-of-mass motion accounts for the fact that a quasi in-plane momentum conservation (which is lost in the case of one QD) is restored, as the exciton states couple to a discrete and yet infinite set of umklapp-photon states. These umklapp states

turned out to be the different photon branches in the reduced zone scheme of the QD lattice Brillouin zone. The resulting umklapp polariton modes have a quantized in-plane motion labelled by the quantum number \mathbf{q} , which is restricted to the 1st BZ. Due to the quasi-momentum conservation a polariton \mathbf{q} is a mixed state of one exciton mode of in-plane momentum \mathbf{q} and a set of photon states with wave vectors $\mathbf{q} + \mathbf{Q}$, where \mathbf{Q} denotes a reciprocal lattice vector. In a good approximation this set of states is finite, as the coupling to large wave vectors is strongly suppressed by an exponential form factor due to the finite size of the dots.

QW polaritons always have a in-plane momentum close to zero due to the steep dispersion of the photon modes [40]. In contrast, in Chapter 3 we demonstrated that in our scheme we can create polaritons with both positive and negative effective masses and a large in-plane momentum at the edge of the Brillouin zone. We calculated that in the majority of cases, namely the cases that have at least a $2\pi/3$ -rotational symmetry, this new type of polariton has an extraordinary small, isotropic effective mass of the order of 10^{-8} electron masses.

We studied the umklapp polariton dispersions for different symmetry points of the square and hexagonal lattice, respectively. In all cases a Rabi splitting of approx. 2 meV was found. Since this value may appear to be very small, we should mention that in II-IV compounds like CdTe, a much larger Rabi splitting at the edge of the Brillouin zone is expected. Moreover in QW's a significant increase of the Rabi splitting can be achieved by the use of stacked layers of QW's. The increase is approximately proportional to the square root of the number of QW's and thus huge values for the QW vacuum field Rabi splitting (in CdTe up to 26 meV) are realizable [2, 39]. The investigation of the effect of stacking layers of QD lattices (i.e. effectively an 3D lattice with small extension in z-direction) could be an interesting project for the future.

Furthermore, we showed in Section 3.5 that the system can be designed in such

a way that the polaritons accumulate in regions where the spontaneous emission lifetime is greatly enhanced due to the inability to fulfill both energy and momentum conservation in the interaction with external photons. We pointed out that for both the positive and negative mass polaritons a population buildup is likely to happen, due to the special dispersion profile and a bottleneck effect.

Certain properties of the umklapp polaritons (as the small mass and the enhanced spontaneous emission lifetime) make them attractive for quantum condensation effects, suggesting very high critical temperatures (Eq. (3.18)). However, we have to stress the fact that the calculations were conducted under the premise of a single excitation and, as we stated above, the presented model only applies to many-body problems, if the lateral exciton confinement does not interfere with the bosonic character of the quasiparticles. Only in this pure bosonic case the statistical properties can be studied exactly. Although Ref. [50] suggests that for a ratio between the dot size and the exciton Bohr radius larger than 5 (for our system we find this ratio to be $\frac{R_Q}{a_B} \approx 10$) the bosonic behaviour is recovered, further investigations are necessary in order to extend our model to a analysis the statistics of a many polariton system.

Another application for the system studied here could be found in the field of quantum information. The natural exciton states are superpositions of localized states on the different QD's

$$|\mathbf{q}\rangle = \sum_i e^{i\mathbf{q}\mathbf{R}_i} |i\rangle. \quad (3.19)$$

Thus in the superposition of multiple polariton states interference effects may lead to a controlled pattern in the occupation of QD's in the lattice. This can be used for a selective entanglement of quantum dot qubit states in the realization of scalable quantum information devices [35, 51].

We conclude that the novel type of quasiparticle called *umklapp polaritons*, which we studied in this thesis, has many properties, which are attractive for both the field of quantum computing and the field of quantum condensation. Further theoretical

as well as experimental investigations of these novel polaritons seem to be interesting and promising research projects for the future.

APPENDICES

APPENDIX A

Derivation of the Effective Mass Equation in Bulk

In the following we are going to show how to derive the effective mass equation (1.18) from the many-body Hamiltonian (1.6)

$$\begin{aligned}
 H_x &= H_0 + H_I \\
 &= \underbrace{\sum_{\mathbf{k}} \left(\Delta + \frac{\hbar^2 k^2}{2m_c} \right) c_{c\mathbf{k}}^\dagger c_{c\mathbf{k}}}_A - \underbrace{\sum_{\mathbf{k}} \frac{\hbar^2 k^2}{2m_v} c_{v\mathbf{k}}^\dagger c_{v\mathbf{k}}}_B \\
 &\quad + \underbrace{\sum_{\mathbf{k}_1 \mathbf{k}_2 \mathbf{k}_3 \mathbf{k}_4} f_{\mathbf{k}_1 \mathbf{k}_2 \mathbf{k}_3 \mathbf{k}_4} c_{v\mathbf{k}_1}^\dagger c_{c\mathbf{k}_2}^\dagger c_{c\mathbf{k}_3} c_{v\mathbf{k}_4}}_C. \tag{A.1}
 \end{aligned}$$

We need to find an equation that the coefficients $A(\mathbf{k}, \mathbf{k}')$ have to fulfill in order to make $|\Psi_x\rangle = \sum_{\mathbf{k}\mathbf{k}'} A(\mathbf{k}, \mathbf{k}') c_{c\mathbf{k}}^\dagger c_{v\mathbf{k}'} |\Phi_0\rangle$ an eigenstate of H_x , i.e $|\Psi_x\rangle$ has to satisfy the stationary Schrödinger equation

$$H_x |\Psi_x\rangle = E |\Psi_x\rangle. \tag{A.2}$$

Therefore we are going to examine the action of H_x on our trial exciton state piece by piece. We start with the part due to conduction electrons A .

$$A |\Psi_x\rangle = \sum_{\mathbf{k}_1} \sum_{\mathbf{k}, \mathbf{k}'} \left(\Delta + \frac{(\hbar \mathbf{k}_1)^2}{2m_c} \right) c_{c\mathbf{k}_1}^\dagger c_{c\mathbf{k}} c_{c\mathbf{k}'}^\dagger c_{v\mathbf{k}'} |\Phi_0\rangle A(\mathbf{k}, \mathbf{k}') \tag{A.3}$$

The product of creation and annihilation operators can be simplified by applying the fermion commutation relations

$$\left[c_{\sigma \mathbf{k}}, c_{\sigma' \mathbf{k}'}^\dagger \right]_+ = \delta_{\mathbf{k}, \mathbf{k}'} \delta_{\sigma, \sigma'}. \quad (\text{A.4})$$

Using these rules we find:

$$c_{c\mathbf{k}_1}^\dagger c_{c\mathbf{k}_1} c_{c\mathbf{k}}^\dagger c_{v\mathbf{k}'} = \delta_{\mathbf{k}_1, \mathbf{k}} c_{c\mathbf{k}_1}^\dagger c_{v\mathbf{k}'} + c_{c\mathbf{k}_1}^\dagger c_{c\mathbf{k}}^\dagger c_{v\mathbf{k}'} c_{c\mathbf{k}_1}. \quad (\text{A.5})$$

If we take into account that the last term on the RHS vanishes, when acting on the ground state $|\Phi_0\rangle$, Eq. (A.3) becomes

$$A |\Psi_x\rangle = \sum_{\mathbf{k}, \mathbf{k}'} \left\{ \left(\Delta + \frac{(\hbar \mathbf{k})^2}{2m_c} \right) A(\mathbf{k}, \mathbf{k}') \right\} c_{c\mathbf{k}}^\dagger c_{v\mathbf{k}'} |\Phi_0\rangle \quad (\text{A.6})$$

To deal with term B we have to simplify a similar term.

$$\begin{aligned} c_{v\mathbf{k}_1}^\dagger c_{v\mathbf{k}_1} c_{c\mathbf{k}}^\dagger c_{v\mathbf{k}'} &= c_{c\mathbf{k}}^\dagger c_{v\mathbf{k}'} + c_{v\mathbf{k}_1} c_{c\mathbf{k}}^\dagger c_{v\mathbf{k}_1}^\dagger c_{v\mathbf{k}'} \\ &= c_{c\mathbf{k}}^\dagger c_{v\mathbf{k}'} + \delta_{\mathbf{k}_1, \mathbf{k}'} c_{v\mathbf{k}_1} c_{c\mathbf{k}}^\dagger - c_{v\mathbf{k}_1} c_{c\mathbf{k}}^\dagger c_{v\mathbf{k}'} c_{v\mathbf{k}_1}^\dagger, \end{aligned} \quad (\text{A.7})$$

where again, the last term produces zero acting on the ground state. With this simplification the action from B on the trial state reads as

$$B |\Psi_x\rangle = \sum_{\mathbf{k}, \mathbf{k}'} \left\{ \left(\sum_{\mathbf{k}_1} \frac{(\hbar \mathbf{k}_1)^2}{2m_v} - \frac{(\hbar \mathbf{k}')^2}{2m_v} \right) A(\mathbf{k}, \mathbf{k}') \right\} c_{c\mathbf{k}}^\dagger c_{v\mathbf{k}'} |\Phi_0\rangle \quad (\text{A.8})$$

The calculation of the third term is slightly more complicated as we have to calculate a product of six operators.

$$c_{v\mathbf{k}_1}^\dagger c_{c\mathbf{k}_2}^\dagger c_{c\mathbf{k}_3} c_{v\mathbf{k}_4} c_{c\mathbf{k}}^\dagger c_{v\mathbf{k}'} |\Phi_0\rangle = -\delta_{\mathbf{k}_3, \mathbf{k}} c_{v\mathbf{k}_1}^\dagger c_{c\mathbf{k}_2}^\dagger c_{v\mathbf{k}_4} c_{v\mathbf{k}'} |\Phi_0\rangle \quad (\text{A.9})$$

The remaining product of four electron operators was already calculated in (A.7) an so we finally find

$$\begin{aligned} C |\Psi_x\rangle &= \sum_{\mathbf{k}, \mathbf{k}'} \sum_{\mathbf{k}_1, \mathbf{k}_2, \mathbf{k}_3, \mathbf{k}_4} f_{\mathbf{k}_1 \mathbf{k}_2 \mathbf{k}_3 \mathbf{k}_4} A(\mathbf{k}, \mathbf{k}') \left\{ \delta_{\mathbf{k}, \mathbf{k}_3} \delta_{\mathbf{k}_1, \mathbf{k}_4} c_{c\mathbf{k}_2}^\dagger c_{v\mathbf{k}'} - \delta_{\mathbf{k} \mathbf{k}_3} \delta_{\mathbf{k}_1 \mathbf{k}'} c_{c\mathbf{k}_2}^\dagger c_{v\mathbf{k}_4} \right\} |\Phi_0\rangle \\ &= \sum_{\mathbf{k}, \mathbf{k}'} \left\{ \sum_{\mathbf{k}_1, \mathbf{k}_2} \left(A(\mathbf{k}_2, \mathbf{k}') f_{\mathbf{k}_1, \mathbf{k}, \mathbf{k}_2, \mathbf{k}_1} - A(\mathbf{k}_1, \mathbf{k}_2) f_{\mathbf{k}_2, \mathbf{k}, \mathbf{k}_1, \mathbf{k}'} \right) \right\} c_{c\mathbf{k}}^\dagger c_{v\mathbf{k}'} |\Phi_0\rangle \end{aligned} \quad (\text{A.10})$$

The first term on the RHS plays the role of a constant, diverging self-energy we are going to suppress in the following. By plugging in the expression for the matrix element f given by (1.5) and by exploiting the fact that the functions $c_{c\mathbf{k}}^\dagger c_{v\mathbf{k}'} |\Phi_0\rangle$ are linearly independent we end up with an equation for the coefficients $A(\mathbf{k}, \mathbf{k}')$ when we put all the three parts together.

$$(E - E_0 - \Delta) A(\mathbf{k}, \mathbf{k}') = \left(\frac{(\hbar\mathbf{k})^2}{2m_c} + \frac{(\hbar\mathbf{k}')^2}{2m_v} \right) A(\mathbf{k}, \mathbf{k}') - \sum_{\mathbf{q}} \frac{4\pi e^2}{\epsilon V q^2} A(\mathbf{k} + \mathbf{q}, \mathbf{k}' + \mathbf{q}) \quad (\text{A.11})$$

By finally introducing the new coefficients

$A_{\mathbf{q}}(\mathbf{K}) := A(\mathbf{K} + (m_c/M)\mathbf{q}, \mathbf{K} - (m_v/M)\mathbf{q})$ we obtain Eq. (1.15).

APPENDIX B

Evaluation of the Interaction Matrix Element

In this appendix we are going to calculate the expression (2.34)

$$X = \sum_{\mathbf{k}_1 \mathbf{k}_2} t_{\mathbf{k}_2, \mathbf{k}_1}^{v, c} A(\mathbf{k}_1, \mathbf{k}_2),$$

in order to complete the exact derivation of the interaction Hamiltonian (2.46) in Section 2.1.3. We carry out the calculation for the E-mode only and present the solution for the M-mode which is obtained in an analogous manner. We start by writing the explicit expression for the matrix element t using the real space representation of the Bloch functions in Eq. (1.3) and the form of the vector potential for the E-mode (Eq. (2.22))

$$\begin{aligned} t_{\mathbf{k}_2, \mathbf{k}_1}^{v, c} &= \langle \mathbf{k}_2 v | \mathbf{A}(\mathbf{r}) | \mathbf{k}_1 c \rangle \\ &= \sum_{\mathbf{q}} \frac{1}{V} \int d\mathbf{r} e^{i(\mathbf{k}_1 - \mathbf{k}_2) \cdot \mathbf{r}} C_{\mathbf{k}} \hat{\epsilon}_E \cos(k_z z) \left(\hat{A}_{\mathbf{k}E}^\dagger e^{-i\mathbf{q}\rho} + \hat{A}_{\mathbf{k}E} e^{i\mathbf{q}\rho} \right) u_{\mathbf{k}_2 v}^*(\mathbf{r}) u_{\mathbf{k}_1 c}(\mathbf{r}), \end{aligned} \quad (\text{B.1})$$

where $C_{\mathbf{k}} = \sqrt{\frac{\hbar}{\epsilon_0 n_r^2 \omega_{\mathbf{k}} V}}$, $\hat{\epsilon}_E = \hat{q} \times \hat{z}$ and as before $\mathbf{r} = (\rho, z)$ and $\mathbf{k} = (\mathbf{q}, k_z)$.

Using the *Rotating Wave Approximation* we can drop the term proportional to $\hat{A}_{\mathbf{k}E}$ because in the Hamiltonian it would appear as a fast oscillating term of the form

$\hat{A}_{\mathbf{k}E}a$. Inserting the latter relation to Eq. (2.34) we find

$$X = \sum_{\mathbf{q}} C_{\mathbf{k}\hat{\epsilon}_E} \hat{A}_{\mathbf{k}E}^\dagger \int d\mathbf{r} \left\{ \frac{1}{V} \sum_{\mathbf{k}_1, \mathbf{k}_2} A(\mathbf{k}_1, \mathbf{k}_2) e^{i(\mathbf{k}_1 - \mathbf{k}_2)\mathbf{r}} \right\} \cos(k_z z) e^{-i\mathbf{q}\rho} u_{\mathbf{k}_2 v}^*(\mathbf{r}) \mathbf{r} u_{\mathbf{k}_1 c}(\mathbf{r}). \quad (\text{B.2})$$

At this point we will exploit the fact that the sum in \mathbf{k} and \mathbf{k}' are restricted to the first Brillouin zone of the quantum dot lattice. This Brillouin zone is very small compared with the crystal Brillouin zone, in which the Bloch functions are defined. In fact for reasonable values for the two lattice constants the volumes of the two zones differ by a factor of approx. 10^9 . Therefore to a very good approximation we can substitute the k dependent Bloch parts by the functions for $\mathbf{k} = 0$

$$u_{\mathbf{k}c(v)}(\mathbf{r}) \approx u_{0c(v)}(\mathbf{r}) \equiv u_{c(v)}(\mathbf{r}) \quad (\text{B.3})$$

Within this approximation the only k dependence is inside the curly braces and one can easily identify this expression as the exciton envelop function taken with the electron and the hole at the same position \mathbf{r}

$$\frac{1}{V} \sum_{\mathbf{k}_1, \mathbf{k}_2} A(\mathbf{k}_1, \mathbf{k}_2) e^{i(\mathbf{k}_1 - \mathbf{k}_2)\mathbf{r}} = \Psi_x(\mathbf{r}, \mathbf{r}) = \chi(\rho) \Phi_{1s}(0) \phi_e(z) \phi_h(z). \quad (\text{B.4})$$

Now, in order to evaluate the remaining integral

$$I = \int d\mathbf{r} \chi(\rho) \Phi_{1s}(0) \phi_e(z) \phi_h(z) \cos(k_z z) e^{-i\mathbf{q}\rho} u_v^*(\mathbf{r}) \mathbf{r} u_c(\mathbf{r}), \quad (\text{B.5})$$

we decompose the integral over the whole space into a sum of integrals over the atomic unit cells as

$$\int d\mathbf{r} = \sum_i \int_{UC} d\mathbf{r}_i, \quad (\text{B.6})$$

where $\mathbf{r}_i = \mathbf{r} - \mathbf{r}_i^0$ and \mathbf{r}_i^0 denotes the i th atom in the crystal. Note that \mathbf{r}_i runs only over a simple crystal unit cell and thus its magnitude has an upper limit defined by the interatomic spacing (≈ 0.1 nm). None of the functions appearing in Eq. (B.5)

changes noticeably within a unit cell except for the Bloch parts u_v^* and u_c .

$$\begin{aligned}
I &= \sum_i \int_{UC} d\mathbf{r}_i \chi(\rho_i^0 + \rho_i) \Phi_{1s}(0) \phi_e(z_i^0 - z_i) \phi_h(z_i^0 - z_i) \cos(k_z(z_i^0 - z_i)) \\
&\quad \times e^{-i\mathbf{q}(\rho_i^0 - \rho_i)} u_v^*(\mathbf{r}_i^0 + \mathbf{r}_i)(\mathbf{r}_i^0 + \mathbf{r}_i) u_c(\mathbf{r}_i^0 + \mathbf{r}_i) \\
&\approx \sum_i \chi(\rho_i^0) \Phi_{1s}(0) \phi_e(z_i^0) \phi_h(z_i^0) \cos(k_z z_i^0) e^{-i\mathbf{q}\rho_i^0} \int_{UC} d\mathbf{r}_i u_v^*(\mathbf{r}_i) \mathbf{r}_i u_c(\mathbf{r}_i), \quad (\text{B.7})
\end{aligned}$$

where we used the periodicity ($u_{c/v}(\mathbf{r}_i^0 + \mathbf{r}_i) = u_{c/v}(\mathbf{r}_i)$) and the orthogonality [13] ($\int d\mathbf{r} u_v^*(\mathbf{r}) u_c(\mathbf{r}) = 0$) of the Bloch functions. The remaining integral is independent of the index i and we define this quantity as

$$\mathbf{u}_{cv} = \frac{1}{V_{UC}} \int_{UC} d\mathbf{r} u_v^*(\mathbf{r}) \mathbf{r} u_c(\mathbf{r}), \quad (\text{B.8})$$

where V_{UC} is the volume of a crystal unit cell. By retransforming the sum into an integral $\sum_i \rightarrow \frac{1}{V_{UC}} \int d\mathbf{r}$ we find

$$I = \Phi_{1s}(0) \tilde{\chi}(\mathbf{q}) I(k_z) \mathbf{u}_{cv}, \quad (\text{B.9})$$

in which we defined $I(k_z) = \int dz \phi_e(z) \phi_h(z) \cos(k_z z)$ and $\tilde{\chi}(\mathbf{q}) = \int d\rho \chi(\rho) e^{-i\mathbf{q}\rho}$. Note that all the information about the position of the dot is contained in $\tilde{\chi}(\mathbf{q}) = \tilde{\chi}_j(\mathbf{q})$.

Gathering the results we finally can write down a compact form for the expression X

$$X = \frac{\hbar}{ie\omega_x} \sum_{\mathbf{q}} \tilde{g}_{\mathbf{k}E}(\mathbf{R}_j) \hat{A}_{\mathbf{k}E}^\dagger \quad (\text{B.10})$$

where we defined the coupling constant

$$\tilde{g}_{\mathbf{k}E}(\mathbf{R}_j) = ie\omega_x \Phi_{1s}(0) \frac{1}{\hbar} C_{\mathbf{k}} \tilde{\chi}_j(\mathbf{q}) I(k_z) (\hat{\epsilon}_E \mathbf{u}_{cv}). \quad (\text{B.11})$$

Note that $\hat{\epsilon}_E \mathbf{u}_{cv}$ is a constant independent of the unit polarization vector $\hat{\epsilon}_E \mathbf{u}_{cv} = u_{cv}$.

In a equivalent calculation one finds the relation between the coupling constants for E- and M-mode to be

$$\tilde{g}_{\mathbf{k}M}(\mathbf{R}_j) = -i \frac{k_z}{k} \tilde{g}_{\mathbf{q}E}(\mathbf{R}_j), \quad (\text{B.12})$$

where we neglected the polarization component perpendicular to the mirrors, as the corresponding coupling term is proportional to

$$I_{\perp}(\frac{\pi}{L}) = \int dz \phi_e(z) \phi_h(z) \sin(\frac{\pi}{L}z), \quad (\text{B.13})$$

and is zero if the z -direction confinement is symmetric. This is equivalent to the statement that in this limit we exclusively couple to excitons that are polarized parallel to the mirrors.

BIBLIOGRAPHY

BIBLIOGRAPHY

- [1] Sadao Adachi. *GaAs, AlAs, and $Al_xGa_{1-x}As$ material parameters for use in research and device applications.* *J. Appl. Phys.*, 58(3):R1–R29, 1985.
- [2] R. Andre, D. Heger, L. S. Dang, and Y. M. d'Aubigne. Spectroscopy of polaritons in CdTe-based microcavities. *J. Cryst. Growth*, 185:758–762, 1998.
- [3] R. Balili, V. Hartwell, D. Snoke, L. Pfeiffer, and K. West. Bose-einstein condensation of microcavity polaritons in a trap. *Science*, 316:1007, 2007.
- [4] G. Barton. Quantum electrodynamics of spinless particles between conducting plates. *Proc. Roy. Soc. A*, 320(1541):251–275, 1970.
- [5] M. Born and K. Huang. *Dynamical Theory of Crystal Lattices*. Clarendon Press, 1954.
- [6] P. Borri, J. R. Jensen, W. Langbein, and J. M. Hvam. Temperature dependence of the polariton linewidth in a GaAs quantum well microcavity. *Phys. Status Solidi B*, 221(1):143–146, 2000.
- [7] Garnett W. Bryant. Excitons in quantum boxes: Correlation effects and quantum confinement. *Phys. Rev. B*, 37(15):8763–8772, 1988.
- [8] R. K. Bullough and B. V. Thompson. Radiation field of molecular crystal. *Journal Of Physics C*, 3(8):1780–&, 1970.
- [9] C. Ciuti, P. Schwendimann, B. Deveaud, and A. Quattropani. Theory of the angle-resonant polariton amplifier. *Phys. Rev. B*, 62(8):R4825–R4828, 2000.
- [10] C. Ciuti, P. Schwendimann, and A. Quattropani. Theory of polariton parametric interactions in semiconductor microcavities. *Semiconductor Science and Technology*, 18(10):S279–S293, 2003.
- [11] C. Cohen-Tannoudji, J. Dupont-Roc, and G. Grynbery. *Photons and Atoms: Introduction to Quantum Electrodynamics*. Wiley & Sons, 1989.
- [12] M. Combescot and C. Tanguy. New criteria for bosonic behavior of excitons. *Europhysics Letters*, 55:390–396, 2001.

- [13] G. Czycholl. *Theoretische Festkörperphysik*. Springer, 2004.
- [14] H. Deng, G. Weihs, C. Santori, J. Bloch, and Y. Yamamoto. Condensation of semiconductor microcavity exciton polaritons. *Science*, 298(5591):199–202, 2002.
- [15] H. Deng, G. Weihs, D. Snoke, J. Bloch, and Y. Yamamoto. Polariton lasing vs. photon lasing in a semiconductor microcavity. *PNAS*, 100(26):15318–15323, 2003.
- [16] U. Fano. Atomic theory of electromagnetic interactions in dense materials. *Phys. Rev.*, 103(5):1202–1218, 1956.
- [17] R. P. Feynman. Simulating physics with computers. *International Journal Of Theoretical Physics*, 21(6-7):467–488, 1982.
- [18] D. Gammon, E. S. Snow, B. V. Shanabrook, D. S. Katzer, and D. Park. Fine structure splitting in the optical spectra of single GaAs quantum dots. *Phys. Rev. Lett.*, 76(16):3005–3008, 1996.
- [19] H. Haug and Stephan W. Koch. *Quantum Theory of the Optical and Electronic Properties of Semiconductors*. World Scientific Publishing Company, 1990.
- [20] J. J. Hopfield. Theory of the contribution of excitons to the complex dielectric constant of crystals. *Phys. Rev.*, 112(5):1555–1567, 1958.
- [21] Kun Huang. On the interaction between the radiation field and ionic crystals. *Proc. Roy. Soc. A*, 208(1094):352–365, 1951.
- [22] A. Imamoglu, R. J. Ram, S. Pau, and Y. Yamamoto. Nonequilibrium condensates and lasers without inversion: Exciton-polariton lasers. *Phys. Rev. A*, 53(6):4250–4253, 1996.
- [23] J. D. Jackson. *Classical Electrodynamics*. Wiley, 1975.
- [24] J. Kasprzak, M. Richard, S. Kundermann, A. Baas, P. Jeambrun, J. M. J. Keeling, F. M. Marchetti, M. H. Szymanska, R. Andre, J. L. Staehli, V. Savona, P. B. Littlewood, B. Deveaud, and L. S. Dang. Bose-einstein condensation of exciton polaritons. *Nature*, 443(7110):409–414, 2006.
- [25] W. Kohn. *Solid State Physics*. chapter 5, page 278. Academic, 1957.
- [26] Arvind Kumar, Steven E. Laux, and Frank Stern. Electron states in a GaAs quantum dot in a magnetic field. *Phys. Rev. B*, 42(8):5166–5175, 1990.
- [27] W. Langbein and J. M. Hvam. Dephasing in the quasi-two-dimensional exciton-biexciton system. *Phys. Rev. B*, 61(3):1692–1695, 2000.

- [28] Otfried Madelung. *Semiconductors: Data Handbook*. Springer, 3 edition, 2004.
- [29] G. D. Mahan and Gustav Obermair. Polaritons at surfaces. *Phys. Rev.*, 183(3):834–841, 1969.
- [30] N. D. Mermin and H. Wagner. Absence of ferromagnetism or antiferromagnetism in one- or two-dimensional isotropic heisenberg models. *Phys. Rev. Lett.*, 17(22):1133–1136, 1966.
- [31] Pierre Meystre and Murray III Sargent. *Elements of Quantum Optics*. Springer, 1999.
- [32] Stanley Pau, Hui Cao, Joseph Jacobson, Gunnar Björk, Yoshihisa Yamamoto, and Atac Imamoglu. Observation of a laserlike transition in a microcavity exciton polariton system. *Phys. Rev. A*, 54(3):R1789–R1792, 1996.
- [33] M. B. Plenio, S. F. Huelga, A. Beige, and P. L. Knight. Cavity-loss-induced generation of entangled atoms. *Phys. Rev. A*, 59(3):2468–2475, 1999.
- [34] Weiming Que. Excitons in quantum dots with parabolic confinement. *Phys. Rev. B*, 45(19):11036–11041, 1992.
- [35] G. F. Quinteiro, J. Fernandez-Rossier, and C. Piermarocchi. Long-range spin-qubit interaction mediated by microcavity polaritons. *Phys. Rev. Lett.*, 97(9):097401, 2006.
- [36] G. Ramon, U. Mizrahi, N. Akopian, S. Braitbart, D. Gershoni, T. L. Reinecke, B. D. Gerardot, and P. M. Petroff. Emission characteristics of quantum dots in planar microcavities. *Phys. Rev. B*, 73(20):205330, 2006.
- [37] M. A. Reed. Quantum dots. *Scientific American*, 268(1):118–123, 1993.
- [38] M. A. Reed, J. N. Randall, R. J. Aggarwal, R. J. Matyi, T. M. Moore, and A. E. Wetsel. Observation of discrete electronic states in a zero-dimensional semiconductor nanostructure. *Phys. Rev. Lett.*, 60(6):535–537, 1988.
- [39] V. Savona, L. C. Andreani, P. Schwendimann, and A. Quattropani. Quantum well excitons in semiconductor microcavities: Unified treatment of weak and strong coupling regimes. *Solid State Commun.*, 93:733–739, 1995.
- [40] V. Savona, Z. Hradil, A. Quattropani, and P. Schwendimann. Quantum-theory of quantum-well polaritons in semiconductor microcavities. *Phys. Rev. B*, 49(13):8774–8779, 1994.

- [41] V. Savona, C. Piermarocchi, A. Quattropani, P. Schwendimann, and F. Tassone. Optical properties of microcavity polaritons. *Phase Transitions*, 68(1):169–279, 1999.
- [42] V. Savona and D. Sarchi. Bose-einstein condensation of microcavity polaritons. *Phys. Status Solidi B*, 242(11):2290–2301, 2005.
- [43] L. J. Sham and T. M. Rice. Many-particle derivation of effective-mass equation for wannier exciton. *Phys. Rev.*, 144(2):708–&, 1966.
- [44] Peter W. Shor. Polynomial-time algorithms for prime factorization and discrete logarithms on a quantum computer. *Siam J. Sci. Statist. Comput.*, 26:1484, 1997.
- [45] D. Snoke. Condensed-matter physics - coherent questions. *Nature*, 443(7110):403–404, 2006.
- [46] M. Sugawara. Theory of spontaneous-emission lifetime of wannier excitons in mesoscopic semiconductor quantum disks. *Phys. Rev. B*, 51(16):10743–10754, 1995.
- [47] M. Sugawara. Theory of exciton spontaneous emission in semiconductor mesoscopic quantum disks embedded in a planar microcavity. *Jpn. J. Appl. Phys.*, 36(4A):2151–2162, 1997.
- [48] F. Tassone, C. Piermarocchi, V. Savona, A. Quattropani, and P. Schwendimann. Bottleneck effects in the relaxation and photoluminescence of microcavity polaritons. *Physical Review B*, 56(12):7554–7563, 1997.
- [49] C. Weisbuch, M. Nishioka, A. Ishikawa, and Y. Arakawa. Observation of the coupled exciton-photon mode splitting in a semiconductor quantum microcavity. *Phys. Rev. Lett.*, 69(23):3314–3317, 1992.
- [50] K. Wójcik, A. Grodecka, and A. Wójs. Quantized absorption strength of multi-exciton quantum dots. *Acta Physica Polonica A*, 110:423–&, 2006.
- [51] W. Yao, R. B. Liu, and L. J. Sham. Theory of control of the spin-photon interface for quantum networks. *Phys. Rev. Lett.*, 95(3):030504, 2005.

MICHIGAN STATE UNIVERSITY LIBRARIES



3 1293 02956 2109